

ALMA MATER STUDIORUM · UNIVERSITÀ DI BOLOGNA

Scuola di Scienze
Corso di Laurea Magistrale in Fisica del Sistema Terra

Definition and classification of Arctic heatwaves

Relatore:
Dott. Paolo Ruggieri

Presentata da:
Giacomo Lorenzi

Sessione III
Anno Accademico 2019/2020

Abstract

The Arctic is warming approximately two time faster than the entire globe, producing considerable local environmental changes that not only affect the fragile Arctic ecosystem but cause also significant socio-economic impacts on the midlatitudes and influence global climate and ocean circulation.

In this context the Arctic warm extremes are receiving a growing attention. Until now they have been studied mostly from a overall point of view, considering their mean characteristics and precursors, or focusing on single particularly intense events.

This thesis work aims to classify them on the base of their large scale circulation features.

Firstly, a definition of *Arctic heatwave* is proposed, combining the methodology used by some recent studies for identifying Arctic warm extremes with the structure common to the majority of the heatwave definitions used in scientific literature.

Then Arctic heatwaves are classified, separately for each season, on the base of their 500-*hPa* geopotential height anomaly maps in the extra-tropical Northern Hemisphere. Particular attention is given to winter extremes.

On the basis of a clustering method, winter events are grouped in three different circulation patterns. Two of these latter are characterized by a pronounced anticyclonic anomaly in the Eurasian sector of the Arctic and by an extensive cold anomaly over southern Siberia (WACE pattern). The third circulation regime is composed by a limited number of events and is countersigned by the prevalence of cyclonic anomalies in the Arctic region. The temporal series of these three regimes shows decadal variations that suggest possible periodicities or Arctic temperature trend dependencies.

In the other seasons the circulation regime with the highest number of heatwaves is characterized by an anticyclonic anomaly over the high Arctic.

Finally, both on a seasonal level and for single regimes a strong positive correlation between heatwave duration and intensity is observed.

Sommario

L'Artico si sta riscaldando a una velocità pressoché doppia rispetto alla media globale, producendo notevoli cambiamenti ambientali che non si ripercuotono solo sul fragile ecosistema artico ma anche sulle attività socio-economiche e commerciali delle medie latitudini, sul clima globale e sulla circolazione oceanica.

In questo contesto gli estremi caldi nell'Artico stanno ricevendo un'attenzione crescente. Fino ad ora sono stati studiati prevalentemente da un punto di vista complessivo, considerando le loro caratteristiche e precursori medi, oppure, al contrario, focalizzandosi su singoli eventi particolarmente intensi.

Questo lavoro di tesi è volto a classificarli in base alle loro configurazioni di circolazione a scala emisferica (tropici esclusi).

Per prima cosa, viene proposta una definizione di *Arctic heatwave* ottenuta combinando la metodologia usata da alcuni recenti studi per identificare gli estremi di temperatura nell'Artico con la struttura comune alla maggioranza delle definizioni di heatwave usate in letteratura.

Successivamente le Arctic heatwave sono classificate, separatamente per ogni stagione, sulla base delle loro mappe (30-90°N) di anomalia dell'altezza di geopotenziale a 500 *hPa*. Un'attenzione particolare è rivolta agli estremi invernali.

Tramite un algoritmo di clustering, gli eventi invernali sono suddivisi in tre diversi regimi di circolazione. Due di essi sono caratterizzati da una pronunciata anomalia anticiclonica nel settore artico euro-asiatico e presentano una estesa anomalia negativa di temperatura sulla Siberia meridionale (WACE pattern). Il terzo regime di circolazione è composto da un numero ristretto di eventi ed è contraddistinto dal prevalere di anomalie cicloniche nell'artico. La serie temporale di questi tre regimi mostra variazioni decadali che suggeriscono possibili periodicità o dipendenze dal trend di temperatura dell'Artico. In ognuna delle altre stagioni il regime di circolazione composto dal maggior numero di eventi è caratterizzato da una anomalia anticiclonica nell'alto Artico.

Infine, sia a livello stagionale che dei singoli regimi si osserva una forte correlazione positiva tra durata e intensità degli eventi.

Contents

1	Introduction	1
1.1	Heatwaves and their definitions	1
1.2	The fast changing climate of the Arctic	9
1.3	Arctic warm extremes: state of the art	16
1.4	This study	21
2	Data and Methods	23
2.1	Heatwave definition	23
2.2	Clustering algorithm	27
2.3	Cross validation procedure	29
3	Results	33
3.1	Winter heatwaves	33
3.2	Spring, Summer and Autumn heatwaves	40
3.3	Heatwave intensity and duration	45
4	Discussion	47
5	Conclusions	51
	Acknowledgements	55
	References	71

1 | Introduction

1.1 Heatwaves and their definitions

Heatwaves (HWs) are periods of abnormally hot weather. Whether they have increased in frequency, duration, and/or amplitude is a much-debated issue in climate science. On a global scale, there is a medium level of confidence that they have increased in frequency and/or duration (IPCC, 2013).

Mean temperature trends may be perceived most through the impacts of extremes, although these are to a large degree dependent on the system under consideration, including its vulnerability, resiliency and capacity for adaptation and mitigation. An extreme weather event becomes a disaster when society and/or ecosystems are unable to cope with it effectively. Growing human vulnerability (due to growing numbers of people living in exposed and marginal areas or due to the development of more high-value property in high-risk zones) is increasing the risk, while human endeavours (such as by local governments) try to mitigate possible effects.

It has been discussed for some time in the climate science literature (Mearns et al. 1984 [72]; Katz and Brown 1992 [54]; Nicholls et al. 1996 [80]; Boer and Lambert 2001 [14]) that small changes in average temperature can result in disproportionately larger changes in the intensity and frequency of extremes. Figure 1.1, extracted from the Intergovernmental Panel for Climate Change (IPCC) Special Report on Extremes (SREX, IPCC, 2012), summarizes how extreme temperature can change in response to a shift in mean temperature, or a change in variability. In many regions, both a shift in mean temperature and variability are reported to be occurring, thus having a combined influence on the increase of hot temperature extremes. Extreme temperature can be categorized in many ways, one of which is heatwaves (HWs).

While the HW definition may vary across different studies (see Section 1.1), a wide consensus exists on the implications of the strongest events on agriculture and land ecosystems (Ciais et al., 2005 [21]), wildfires and air pollution (Vautard et al. 2005 [130]), human comfort and mortality (WHO 2004 [58] 2010 [83]), and power shortages (Fink et al. 2004 [33]), amongst others.

Persistent periods of very high temperature have a strong impact on human health (Tomczyk and Bednorz 2016 [125]). In 2003, an intense heatwave occurred over Western

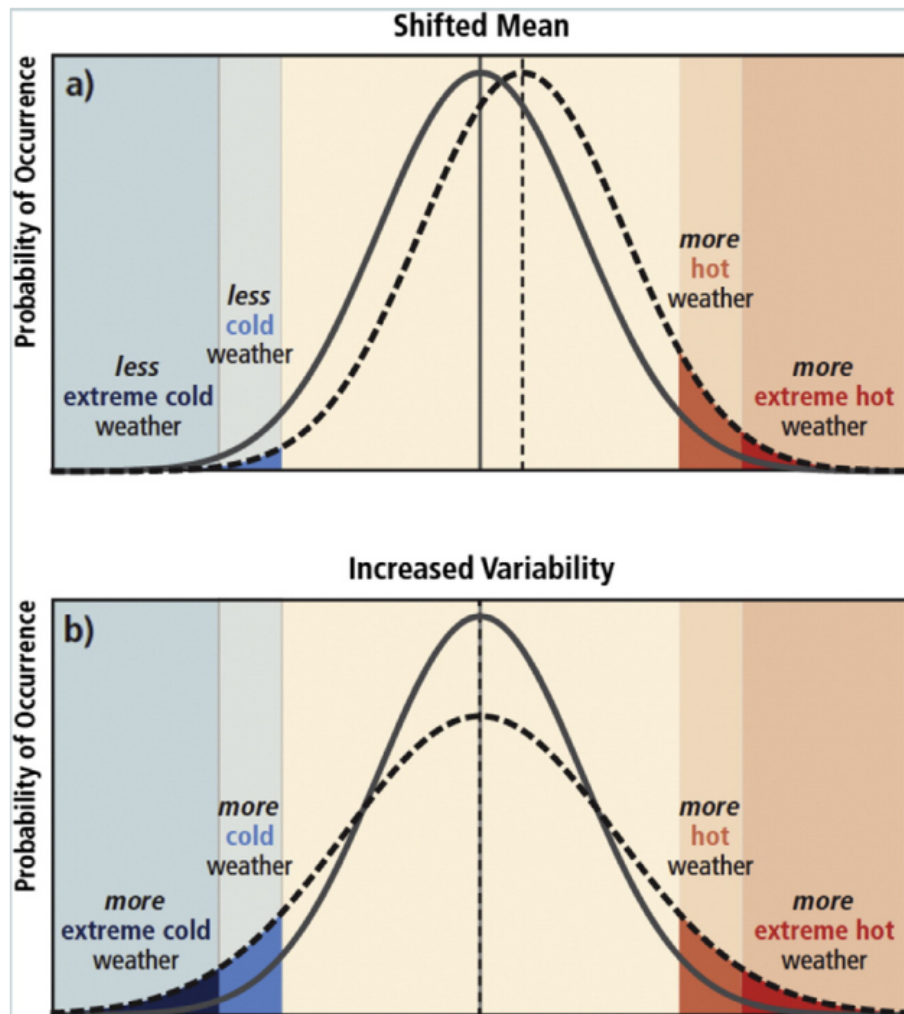


Figure 1.1: Schematics showing changes in extreme temperature in relation to shifts in average temperature (a) and variability (b). The gray curve represents the current climate, the black dashed curve represents a climate with the respective shift. Note that a shift in the mean infers higher frequencies of hot weather, as well as hot extremes that were extremely rare in the original distribution. A shift in variability only can result in extremes in both hot and cold weather. Adapted from Figure SPM.3 of IPCC (2012) by Perkins 2015 [92].

Europe, with temperatures the highest since 1500 (Luterbacher et al. 2004 [67]). This event was responsible for over 70 000 deaths (Coumou and Rahmstorf 2012 [24]). The 2010 Russian heatwave, which lasted over a month, killed around 54 000 individuals (McMichael and Lindgren 2011 [71]). In 2009 a heatwave over south eastern Australia had been associated with 374 human deaths, double that of the bushfire that followed

(Victorian Department of Health 2009). Indeed, heatwaves have been dubbed the “silent killer”, as they generally exacerbates underlying medical conditions. Thus it is likely that the true number of heatwave-related deaths is underestimated Perkins 2015 [92]. Moreover, it is not necessarily the daytime heat which is always responsible for morbidity and mortality, humans need lower nighttime temperatures to recuperate. In the most extreme heatwaves, such as the 2003 European heatwave, nighttime temperatures were abnormally high, which contributed largely to the final death toll (Trigo et al. 2005 [126]).

Another system adversely impacted by heatwaves is human infrastructures. Heat waves may physically damage electricity infrastructures (Depietri et al. 2012 [27]), causing problems for both energy generation and transmission (Matzarakis and Nastos 2011 [69]). Australian heatwaves have caused railways to buckle (McEvoy et al. 2012 [70]) and put an enormous strain on power supply (Colombo et al. 1999 [23]), having knock-on effects to human health (e.g. Wrigley et al. 2006 [140]). Parts of the United States are projected to fall short of the required energy load by almost 20%, with increasing temperature extremes in the future mapped on to current infrastructures (Miller et al. 2008 [74]). Future trends in heat waves may also influence the supply of water. Runoff production and river discharge is expected to be anti-correlated with anomalous hot weather (this was confirmed by Zampieri et al. 2016 [142] for the Alpine region). In fact, heat waves cause an increase of evapo-transpiration that reduces soil moisture, and soil moisture deficit itself can act as an amplifier of heat waves amplitude (see e.g. Seneviratne et al. 2010 [116]; van den Hurk et al. 2011 [127]) inducing a positive feedback. The combined surface temperature warming and the reduction in water availability during HWs showed the vulnerability of the energy sector in Europe and around the world (van Vliet et al. 2013 [129]; Scanlon et al. 2013 [111]; Koch and Voge 2009 [57]).

Agricultural industries are also adversely impacted by extreme heat. Russian grain harvests suffered a loss of 30% after the 2010 event (Barriopedro et al. 2011 [10]), due to sensitive tolerances that affect grain filling and reproduction (Barlow et al. 2013 [8]). Other crops such as rice are also impacted by extreme temperatures (Lanning et al. 2011 [60]), as are bovine livestock and their milk production (Dunn et al. 2014 [30]).

Natural ecosystems are also finely in tune with their surrounding habitats, and are generally only tolerant to specific temperatures. Whole terrestrial ecosystems (as well as human property) are also at risk of increased fire danger during and directly after a heatwave. The intense temperatures further exacerbate the drying of vegetation, which, due to preceding conditions, is likely already very dry. Thus, the likelihood of combustion after ignition is increased [92]. This is extremely evident in the recent numerous and extended wildfires over Siberia, Australia and California.

It is also worth remembering that heatwaves are not restricted to land, they can also occur in the ocean. A marine heatwave over Western Australia in 2010/2011 caused catastrophic damage to local seaweed populations, and the first-ever coral bleaching event on the local reefs (Smale and Wernberg 2013 [119]; Wernberg et al. 2013 [134]). A 2012

Marine heatwave in the northwest Atlantic seriously impacted local fish species, inducing concern of increased frequency of similar events as the global climate continues to warm (Mills et al. 2013 [75]).

Not only HW in summer periods, but also warm spells during coldest months can have marked consequences for environmental and socioeconomic systems, especially those warm spells in regions where snow has a major influence on the economy, ecology, and water availability (Beniston, 2005 [11]). Thus, HW periods during winter have been shown to cause floods, result in poor skiing conditions, and disrupt crop production (Shabbar and Bonsal 2003 [117]; Beniston et al. 2007 [12]). In Sierra Nevada (south of Spain) winter snow accumulation controls more than 40% of the spring runoff, which determines the capability to fill the reservoirs which supply water for large irrigation areas in the Alpujarras Guadalfeo Valley, and permits ski tourism, which is currently the main economic activity of that area. Thus, an increase in the frequency and magnitude of warm spells could have particular importance for the hydrology and economy of the region (Barcena-Martin et al. 2019 [7]).

Therefore, heatwaves can involve devastating impacts in all season and in different areas (from natural ecosystems to energy infrastructure, from human health to several economic sectors), and the scientific and public concern about them is increasing in a global warming and population growing scenario.

The next part of this Section shows an overview of the several ways to measure them and focuses on the main methods.

There are many ways to define a heat event, and what constitutes one can vary considerably depending on the meteorological variables or impacts of interest (Horton et al. 2016 [50]). Temperature is often the only quantity used in heat event definitions due to its nearubiquitous measurement; moisture is rarely incorporated despite its strong correlation with thermal stress in humans and other large mammals (e.g. Davis et al. 2016 [26]). While three heat event metrics—magnitude, duration, and frequency—are of general importance, the myriad ways to define heat events imply that there are no simple answers to definitional questions about event thresholds (“what magnitude temperature anomaly is required?”) or scope (“over what spatial and temporal scales?”). Another major distinction concerns definitions based on absolute temperatures versus percentiles. Absolute temperatures are of central importance for many societal and environmental impacts, such as the biophysical heat tolerances of mammals or the resilience of infrastructure. Therefore many national meteorological agencies (e.g. Netherlands’ and China’s ones) issue warnings to health services when absolute thresholds are predicted to be exceeded, as reported in Barcena-Martin et al. 2019 [7]. In the United States, the National Weather Service suggests early warning when the daytime heat index (including adjustment for humidity) reaches 40.6 °C and a night-time minimum temperature of 26.7 °C persists for at least 48 hr (Gershunov et al., 2009 [38]).

Percentiles relative to the local climatology facilitate comparisons across locations and

over time given differences in tolerance and preparedness (e.g. Anderson and Bell 2009 [2]), and when model and observational climatologies differ. For this reason percentile threshold are the most common approach used in climatology.

Such a multitude of definitions points to a need for more work on creating a standardized set, foremost to facilitate inter-study comparison and to increase sample sizes of upper-tail temperature events given large natural variability. Under the aegis of the World Climate Research Programme, an extremes standardization for observations and reanalysis is underway, motivated by the strict requirements of detection and attribution. The Expert Team on Climate Change Detection and Indices (ETCCDI) has defined 27 internationally-agreed indices of climate extremes (17 of which measure extreme temperature) based on daily data. This list includes a variety of percentile, absolute threshold, duration, and range-based temperature indices (see Figure 1.2). The ETCCDI indices have been, and still are, widely applied to observational and climate model data to understand previous and future changes in extreme events.

Index shorthand	Characteristic measured & timescales	Index definition
TN10p	Frequency; monthly & annual	Occurrence of cold nights (daily minimum temperature) below the 10th percentile
TN90p	Frequency; monthly & annual	Occurrence of warm nights above the 90th percentile
TX10p	Frequency; monthly & annual	Occurrence of cold days (daily maximum temperature) below the 10th percentile,
TX90p	Frequency; monthly & annual	Occurrence of warm days above the 90th percentile.
TXx	Intensity; monthly & annual	Maximum daily maximum temperature
TNx	Intensity; monthly & annual	Maximum daily minimum temperature
TXn	Intensity; monthly & annual	Minimum daily maximum temperature
TNn	Intensity; monthly & annual	Minimum daily minimum temperature
FD	Frequency; annual	Occurrence of frost days (minimum temperature below 0 °C)
ID	Frequency; annual	Annual occurrence of ice days (maximum temperature below 0 °C)
SU	Frequency; annual	Annual occurrence of summer days (maximum temperature above 25 °C)
TR	Frequency; annual	Annual occurrence of tropical nights; (minimum temperature above 20 °C).
CSDI	Duration; annual	Cold spell duration indicator (count of days part of a 6-day window when minimum temperature is below the 10th percentile)
WSDI	Duration; annual	Warm spell duration indicator (count of days part of a 6-day window when maximum temperature is above the 90th percentile)
GSL	Duration; annual	Growing season length (as defined by Frich et al., 2002)
DTR	Range/spread; monthly	Diurnal temperature range (monthly mean difference between daily maximum and minimum temperature)
ETR (no longer part of ETCCDI framework)	Range/spread; monthly	Extreme temperature range (as defined by Frich et al., 2002)

Figure 1.2: 17 measures of extreme temperature proposed by ETCCDI (taken from Perkins 2015 [92]).

Our review reveals that the majority of HW definition in scientific literature share the same structure:

1. consider a daily temperature variable;
2. use a percentile threshold to be exceeded by the variable;
3. request a minimum number of consecutive days above the threshold.

The chosen variable is often the daily maximum temperature (Fischer and Schär 2010 [34]; Perkins and Alexander 2012 [93]; Photiadou et al. 2013 [98]; Russo et al. 2014 [107], 2015 [108]; Rohini et al. 2016 [105]; Zampieri et al. 2016 [142]; Zschenderlein et al.

2019 [144]; Barcena-Martin et al. 2019 [7]; Zhang et al. 2020 [143]; Perkins-Kirkpatrick and Lewis 2020 [94]). Perkins and Alexander 2012 [93] propose also the minimum daily temperature. Parker et al. 2013 [90], Quinting and Reeder 2017 [101] and Barcena-Martin et al. 2019 [7] request a double condition considering both maximum and minimum daily temperature. Finally, Messori et al. 2018 [73] used daily mean temperature anomaly, whereas Reis et al. 2019 [104] used daily maximum temperature anomaly.

The majority of definition adopt the 90th*pct*, but also the 95th*pct* is common (e.g. Stefanon et al. 2012 [122] and Barcena-Martin et al. 2019 [7]). A crucial step of the definition is the decision of the set of values from which the percentile is calculated. The most common design is the collection of all the x -day running window (possible values of x are 3, 15, 21, 31) belonging to a fixed (in most cases) or moving (e.g. Barcena-Martin et al. 2019 [7]) set of years. Obviously if the set of years is fixed (in which case is called ‘reference period’) climatological trends in mean temperature affect the measure of heatwave frequency and intensity. The x -day running window allows to account for the seasonal cycle.

In some cases, instead of the x -day running window, the monthly climatology is used (e.g. Parker et al. 2013 [90]; Quinting and Reeder 2017 [101]).

The minimum temporal duration is set on the base of the purpose of the study and on the climate variability of the region of interest. However the most common threshold is 3 days (Perkins and Alexander 2012 [93]; Parker et al. 2013 [90]; Rohini et al. 2016 [105]; Barcena-Martin et al. 2019 [7]; Perkins-Kirkpatrick and Lewis 2020 [94]), but also 4 (Stefanon et al. 2012 [122]; Zhang et al. 2020 [143]), 5 (Spensberger et al. 2020 [121]) and 6 (Fischer and Schär 2010 [34]; Matthes et al. 2015 [68]) are used.

Typically heatwaves have a considerable spatial extent (hundreds of thousand km^2) in accordance with the synoptic-scale nature of its drivers (typically a quasi-stationary high-pressure system [92]). Many studies do not include a spatial extent criterion in the definition of heatwaves. On the other hand, for those studies that impose a large-scale requirement the two most usual approaches are to apply the aforesaid definition to the temperature variable averaged over the region of interest (e.g. Reis et al. 2019 [104]; Perkins-Kirkpatrick and Lewis 2020 [94]) or to require the conditions to be satisfied over a certain percentage of the study domain (e.g. Spensberger et al. 2020 [121]).

Here different definitions of HW adopted in scientific literature are reviewed to better identify similarities and differences among them.

First, the definition adopted by Stefanon et al. 2012 [122], tailored to study European and Mediterranean heatwaves, is reported. For a given day d at a given grid-point, the threshold is the 95th percentile of the set of data A_d defined by:

$$A_d = \bigcup_{y=1950}^{2009} \bigcup_{i=d-10}^{d+10} T_{y,i}$$

where \cup denotes the union of sets and $T_{y,i}$ is the local temperature value for day i of year

y .

Furthermore, taking a square of side $L=3.75^\circ$ (in latitude and longitude), there must be at least a fraction $\alpha=0.6$ of the surface where the temperature exceeds the 95th percentile, using weights on the cosine of latitude. In this case, the central point of the square is retained as a heatwave point.

The above criteria are to be satisfied over at least four consecutive days. The temporal criterion is applied counting also adjacent regions. More precisely, when two heatwave squares overlap by more than 40% of their surface, they are retained as one single coherent event. This criterion allows to smooth off some of the intermittency in the temperature signal, as well as to account for propagating phenomena.

This articulated definition allows to give a spatial representation of the heatwaves suited for further pattern analyses and classifications (see Figure 1.3).

Another significant definition of heatwaves is that created by Russo et al. 2015 [108] because it has a typical structure and because is linked with by the definition of a magnitude index (HWMId). Both definitions were used by successive studies (Zampieri et al. 2016 [142]; Zschenderlein et al. 2019 [144]). Heatwaves are indicated as period ≥ 3 consecutive days with maximum temperature (Tmax) above the daily threshold for the reference period 1981–2010. The threshold is defined as the 90th percentile of daily maxima temperature, centered on a 31 day window. Hence, for a given day d , the threshold is the 90th percentile of the set of data A_d defined by:

$$A_d = \bigcup_{y=1981}^{2010} \bigcup_{i=d-15}^{d+15} T_{y,i}$$

where $T_{y,i}$ is the daily maximum temperature value for day i of year y . Moreover, the Heatwave magnitude index daily (HWMId) is the sum of the magnitude of the consecutive days composing a heatwave, with daily magnitude calculated as follow:

$$M_d = \begin{cases} \frac{T_d - T_{30y25p}}{T_{30y75p} - T_{30y25p}} & \text{if } T_d > T_{30y25p} \\ 0 & \text{if } T_d \leq T_{30y25p} \end{cases}$$

with T_d being the maximum daily temperature on day d of the heatwave, T_{30y25p} and T_{30y75p} are, the 25th and 75th percentile values, respectively, of A_d .

So HWMId is an adimensional index that increases with increasing HW duration and intensity, and that allows to compare events of regions with different climate variance.

To conclude, Barcena-Martin et al. 2019 [7] proposed three different definitions of heatwave in order to substitute the simplistic AEMET (Spain's State Meteorological Agency) and IPCC definitions (see [7] for these last two). According to the first of the three definitions, called MRDT (moving reference period and daily threshold), an HW is a period ≥ 3 consecutive days with daily maximum temperature above its 95th percentile

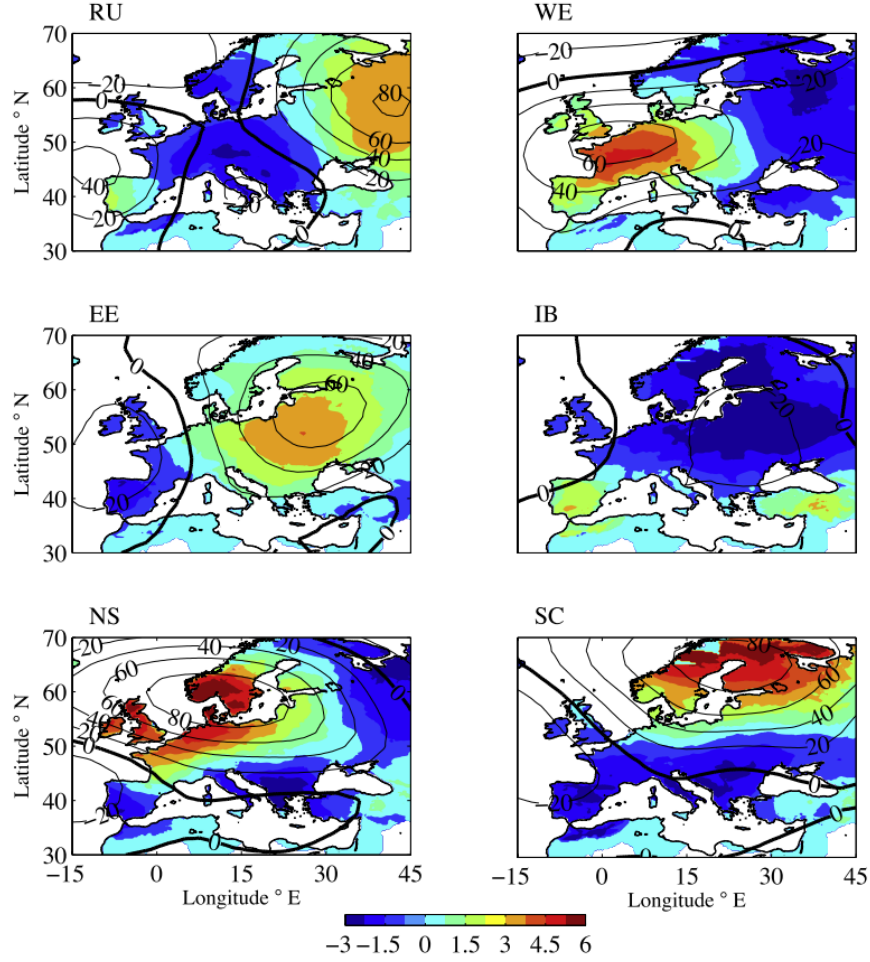


Figure 1.3: Six heatwave patterns obtained by Stefanon et al. 2012 [122] using a hierarchical clustering algorithm for the Euro-Mediterranean region. Daily maximum temperature anomalies are in color and expressed in deg K and isolines are the 500- hPa geopotential height anomaly. Taken from Stefanon et al. 2012. [122].

calculated for a given day d at a given year y from set of data A_{dy} defined by:

$$A_{dy} = \bigcup_{j=y-30}^{y-1} \bigcup_{i=d-1}^{d+1} T_{j,i}$$

where $T_{j,i}$ is the daily maximum temperature value for day i of year j . This threshold varies not only with the Julian day but also with the year, detrending de facto the threshold and updating it to current (lagged-)conditions. The ~ 15 -yr back lag allow to calculate the thresholds for the current year permitting an in-time operational use. Due to the fact that an elevated by-night temperature is also a key health risk factor the

other two alternative definitions are based on a moving reference period and two daily thresholds (for T_{max} and T_{min}) and therefore are named as MR2DT. According to the MR2DT(OR), a HW is a period of at least three consecutive days in which the T_{max} is above the 95th percentile of the series of daily T_{max} for the specific Julian day, or in which the T_{min} is above the 95th percentile of the series of daily T_{min} for the specific Julian day. In the same line, MR2DT(AND) imposes that both thresholds should be exceeded simultaneously. From this overview it can be concluded that the majority of studies dealing with warm extremes were conducted on mid-latitude regions. This is reasonably explained by the many aforementioned impacts of heat waves on densely populated regions. The following section discusses the fast changing climate of the Arctic, introducing the concept of Arctic Amplification, and demonstrate that impacts on human activities in the Arctic regions are likely to increase.

1.2 The fast changing climate of the Arctic

This Section offers an overview of some of the main issues raised by the rapid climate evolution the Arctic is facing.

One of the most evident manifestations of recent climate change is Arctic amplification— that is, surface warming over the Arctic being faster than that at other latitudes under greenhouse warming (IPCC 2013). Such amplification has accelerated in recent decades and the Arctic has warmed approximately twice as rapidly as the Northern Hemisphere (NH) as a whole (Cohen et al. 2014 [22]).

The cause of the 'fast' Arctic warming remains a controversial issue and several important factors have been suggested, including the following: surface reflectivity of snow and ice (Arrhenius 1896 [4]), oceanic heat loss by surface turbulent heat fluxes (Carmack and Melling 2011 [15]), incoming longwave radiation emitted by water vapor and clouds (e.g. Francis and Hunter 2007 [36]), surface thermal inversion (Bintanja et al. 2011 [13]), atmospheric lapse-rate (Pithan and Mauritsen 2014 [99]; Graverson et al. 2014 [42]), and poleward atmospheric energy transport by moisture intrusion (Park et al. 2015 [87]; Woods and Caballero 2016 [137]; Graverson and Burtu 2016 [41]). These local and remote factors are not independent nor mutually exclusive and should collectively contribute to Arctic warming.

One of the most evident effect (and, in turn, cause) is the reduction of Arctic sea ice, that occurred in all seasons during recent decades. The largest decline in areal extent have occurred during summer and early autumn (up to 10% $decade^{-1}$), but the thicker multiyear ice cover is shrinking rapidly in winter as well (Sorokina et al. 2016 [120]). Sea-ice loss contributes to the Arctic Amplification especially because of the ice–albedo feedback. This latter mechanism arises from the fact that for shortwave radiation the ice reflectivity is much higher than the ocean (and land) one. Hence, as ice cover decreases, more incoming solar radiation is absorbed by the surface that warms, causing further ice

melting.

With increasing ice-free regions shipping activities are expanding in the Arctic and aim toward a range of goals, including the assessment and extraction of Arctic marine resources, such as fisheries, minerals, oil and gas, and surveys, tourism and the investigation of transport along new shipping routes across the Arctic from Asia to Europe and North America (Figure 1.4). According to Schøyen and Bråthen 2011 [113], the exploitation of shipping routes in the Arctic Ocean can, in principle, reduce the navigational distances between Europe and Asia by about 40%, decreasing sailing time and saving fuel (with a consequent considerable reduction of CO_2 emissions). Average sailing times on the North Sea Route (NSR), also called Northeast Passage (red in Figure 1.4), have fallen from 20 days in the 1990s to 11 days in 2012–2013, attributed to easing sea ice conditions along the Siberian coast (Aksenov et al. 2017 [1]). Moreover, Eguiluz et al. 2016 [32] provided quantitative evidence that the extent of Arctic shipping in the period 2011–2014 was already significant. It is mostly concentrated in the Norwegian and Barents Seas, and predominantly accessed via the Northeast and Northwest Passages (respectively red and violet in Figure 1.4), whereas thick ice prevents transit along the direct trans-Arctic route (yellow in Figure 1.4). But this latter is foreseen to be viable during the summer season by the mid 21st century [32].

Therefore, Arctic sea-ice decline is forecasted to shift global shipping traffic, requiring the development of infrastructures and governance arrangements and the management of risks to marine life and ecosystems (Eguiluz et al. 2016 [32]).

The Arctic is relevant also for its peculiar ecosystem that enhances Earth biodiversity and allows the subsistence of the Inuit communities. Community-based studies across the Canadian Arctic have identified several widespread vulnerabilities (Pearce and Smit 2013 [91]). Subsistence hunting is susceptible to changes in wildlife populations and access to hunting areas; changes in the availability of harvested food contribute an additional risk to people's health; the erosion of environmental knowledge and land skills enhances the vulnerability of Inuit hunters to climate risks [91].

Another important phenomenon to deal with is thermokarst, that is the process whereby the thawing of ice-rich permafrost ground causes land subsidence. Accelerated thermokarst due to Arctic warming has implications for community infrastructures and for coastal erosion [91], but also impacts hydrology, ecology and biogeochemistry (Olefeldt et al. 2016 [82]; Schaefer et al. 2020 [112]). Thermokarst landscapes are estimated to cover $\sim 20\%$ of the northern boreal and tundra circumpolar permafrost region (Figure 1.5), and to store approximately half of the below-ground organic carbon within this region [82]. Therefore it is necessary to explicitly considering thermokarst when assessing impacts of climate change, including future landscape greenhouse gas emissions [82].

Since the 1970s, historically unprecedented changes have been observed in the Arctic as climate warming has increased precipitation, river discharge, and glacial as well as sea-ice melting. In addition, modal shifts in the atmosphere have altered Arctic Ocean



Figure 1.4: Principal shipping routes in the Arctic: the Northwest Passage (violet), the Northeast Passage (red) and the direct trans-Arctic route (yellow). Anchors denotes the ports already present along the routes (with violet background for the Northwest Passage and red background for the Northeast Passage) and the planned ones (with yellow background for the trans-Arctic route). Taken from *Limes*, the Italian journal of geopolitics (<https://www.limesonline.com/cartaceo/londra-mette-lartico-nel-mirino>).



Figure 1.5: Maps showing the carbon-rich regions subject to thermokarst. Taken from Nature 569, 32-34 (2019) (DOI: <https://doi.org/10.1038/d41586-019-01313-4>).

circulation patterns and the export of freshwater into the North Atlantic (Greene et al. 2008 [44]). Since the early 1990s, these processes have been associated with two types of ecological responses in the North Atlantic. The first of these responses has been an ongoing series of biogeographic range expansions by boreal plankton (Sundt and Melle 1998 [123]; Johns et al. 2001 [52]; Reid and Beaugrand 2002 [102]; Greene and Pershing 2007 [43]; Reid et al. 2007 [103]), including renewal of the trans-Arctic exchanges of Pacific species with the Atlantic. The second response was a dramatic regime shift in the shelf ecosystems of the Northwest Atlantic that occurred during the early 1990s (Greene and Pershing 2007 [43]). This regime shift resulted from freshening and stratification of the shelf waters, which in turn could be linked to changes in the abundances and seasonal cycles of phytoplankton, zooplankton, and higher trophic-level consumer populations (Durbin et al. 2003 [31]; Pershing et al. 2005 [95]).

It is predicted that the recently observed ecological responses to Arctic climate change in the North Atlantic will continue into the near future. It is more difficult to predict ecological responses to abrupt climate change in the more distant future as tipping points in the Earth's climate system are exceeded (Greene et al. 2008 [44]).

In this regard Armitage et al. 2020 [3] highlighted a critical situation. According to them, since the 1990s the Beaufort Gyre has accumulated a large amount of fresh water (8000 km^3 , almost twice the volume of Lake Michigan). The cause of this gain in freshwater concentration is the loss of sea ice in summer and autumn. This decades-long decline of the Arctic's summertime sea ice cover has left the Beaufort Gyre more exposed to the wind, which spins the gyre faster and traps the fresh water in its current. Persistent westerly winds have also dragged the current in one direction for over 20 years, increasing the speed and size of the clockwise current and preventing the fresh water from leaving the Arctic Ocean. This decades-long western wind is unusual for the region, where previously, the winds changed direction every five to seven years. If the direction were to change, the wind would reverse the current, releasing the fresh water it has accumulated into the Atlantic Ocean. This event could potentially slow down Atlantic circulation. And that would have hemisphere-wide implications for the climate, especially in Western Europe. Indeed the Atlantic Meridional Overturning Circulation helps regulate the planet's climate by carrying heat from the tropically-warmed water to northern latitudes. If slowed enough, it could negatively impact marine life and the communities that depend on it.

Armitage et al. 2020 [3] also found that, although the Beaufort Gyre is out of balance because of the added energy from the wind, the current expels that excess energy by forming small, circular eddies of water. While the increased turbulence has helped keep the system balanced, it has the potential to lead to further ice melt because it mixes layers of cold, fresh water with relatively warm, salt water below. The melting ice could, in turn, lead to changes in how nutrients and organic material in the ocean are mixed, significantly affecting the food chain and wildlife in the Arctic. These results reveal a delicate balance between wind and ocean as the sea ice pack recedes under climate

change.

But not only the long trend of Arctic warming has great effect on Arctic and North Atlantic ecosystems but also temperatures extremes. For example, in summer 2008 extreme warming was recorded at Ward Hunt Island and vicinity, the northern limit of the Canadian high Arctic, with air temperatures up to 20.5 °C. This was accompanied by pronounced changes in microbial habitats: deepening of the permafrost active layer; loss of perennial lake ice and sea ice; loss of ice-dammed freshwater lakes; and 23% loss of total ice shelf area, including complete break-up and loss of the Markham Ice Shelf cryo-ecosystem (Vincent et al. 2009 [131]). This involves the decline in the habitat of polar bears and ringed seals, as well as shifts in phytoplankton structure and bloom timing (Post et al. 2013 [100]; Woelders et al. 2018 [136]).

These observations underscore the vulnerability of Arctic ecosystems to extreme weather and a changing climate.

A growing number of studies on the connection between Arctic and mid-latitude climates, particularly on temperature extremes, were conducted in the last decades (e.g. Cohen et al. 2014 [22]). They are briefly reviewed hereafter.

A number of unusually harsh cold winters have occurred in many parts of East Asia and North America in the past few years (e.g. Wang and Chen 2014 [133]; Van Oldenborgh et al. 2015 [128]), and observational and modelling studies have suggested that atmospheric variability linked to Arctic warming might have played a central role (e.g. Outten and Esau 2012 [84]; Screen and Simmons 2014 [115]; Francis and Vavrus 2015 [37]). Figure 1.6 shows how from the late 90's during the winter season a strong arctic warming corresponded to a negative temperature trend over continental mid-latitudes.

The North/South temperature gradient is an important driver of the polar jet stream, thus as rapid Arctic warming continues, one anticipated effect is a slowing of upper-level zonal winds (Francis and Vavrus 2015 [37] provided evidence in that sense). It has been hypothesized that these weakened winds would cause the path of the jet stream to become more meandering, leading to slower Eastward progression of ridges and troughs, which increases the likelihood of persistent weather patterns and, consequently, extreme events (Screen and Simmons 2014 [115]).

Kug et al. 2015 [59] found that severe winters across East Asia are associated with anomalous warmth in the Barents–Kara Sea region, whereas severe winters over North America are related to anomalous warmth in the East Siberian–Chukchi Sea region. Moreover, they stated that each regional warming over the Arctic Ocean is accompanied by the local development of an anomalous anticyclone and the downstream development of a mid-latitude trough. The resulting northerly flow of cold air provides favourable conditions for severe winters in East Asia or North America [59]. These links between Arctic and mid-latitude weather are also robustly found in idealized climate model experiments and CMIP5 multi-model simulations [59].

Eurasia has recently experienced some anomalous winters with severe cold spells, particu-

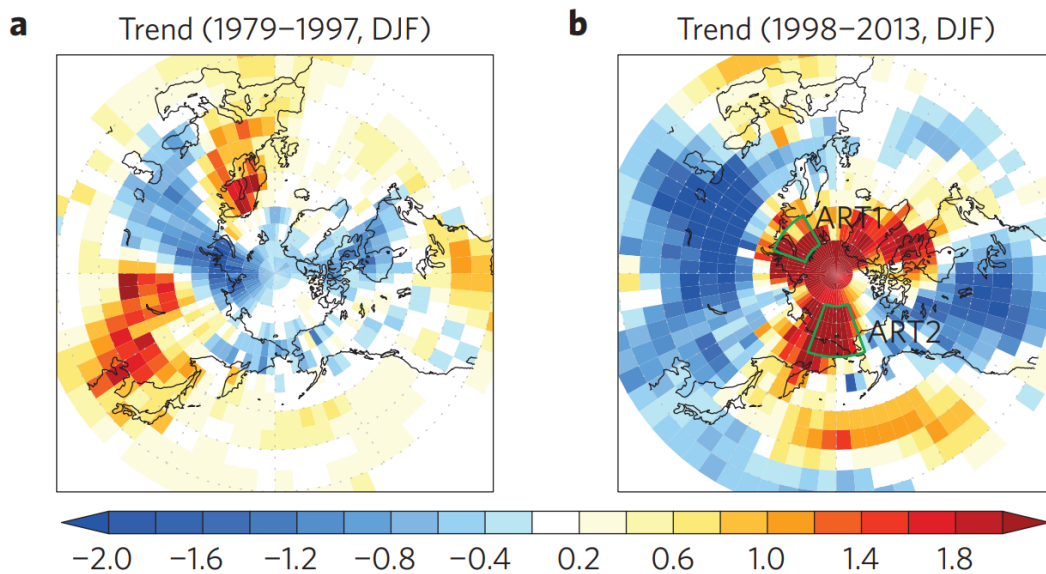


Figure 1.6: The linear trend in surface air temperature during December–February for the periods 1979/1980–1997/1998 (a) and 1997/1998–2013/2014 (b) from the observed data. Taken from Kug et al. 2015 [59].

larly strong over central Siberia, and above-normal snow cover. This phenomenon has been termed ‘warm Arctic–cold Siberia’ (WACS) or ‘warm Arctic–cold Eurasia’ (WACE) (Overland et al 2011 [85]; Inoue et al 2012 [51]). Various mechanisms have been proposed to explain how the WACS pattern is generated. Early on, Honda et al. 2009 [48] pointed to the fact that, where sea ice retreats, we expect enhanced ocean-to-atmosphere energy loss in the form of turbulent heat fluxes (THFs). They suggested that such a THF perturbation triggers a stationary Rossby wave train that amplifies the climatological mean wintertime high pressure over Siberia and enhances northerly cold-air advection over eastern Eurasia. Other studies focus on the role of the THF perturbation in modifying the near-surface meridional temperature gradient, leading to altered cyclone pathways and a cold anticyclonic flow anomaly north of the Eurasian continent (Inoue et al 2012 [51]), or weakened zonal winds and reduced heat transport from the North Atlantic to the interior of the Eurasian continent (Petoukhov and Semenov 2010 [96]; Outten and Esau 2012 [84]).

A different class of studies examines the phenomenon of cold Eurasian winters independently of Arctic sea ice. These studies attribute cold winters to high latitude blocking but not necessarily in connection with declining ice cover. Wintertime blocking patterns in recent cold years (e.g. 2005/06, 2009/10) are shown to be linked to sudden stratospheric warmings and/or sea surface temperature anomalies (Scaife and Knight 2008 [110]; Croci-Maspoli and Davies 2009 [25]; Cattiaux et al. 2010 [16]), with Rossby wave trains playing a possible amplifying role over Siberia (Takaya and Nakamura 2005 [124]; Park et al. 2011

[89]; Cheung et al. 2013 [19]; Sato et al. 2014 [109]). While such atmospheric circulation changes could be forced by sea ice changes (Mori et al. 2014 [77]), they could also be an expression of natural internal variability or reflect a direct atmospheric response to external radiative forcing.

Most recently, a series of observational and modeling studies has questioned whether there is adequate evidence that sea ice influences atmospheric circulation, blocking, and Eurasian winter temperatures at all (Hopsch et al. 2012 [49]; Screen and Simmonds 2013 [114]; Barnes et al. 2014 [9]; Wallace et al. 2014 [132]; Woollings et al. 2014 [139]).

Sorokina et al. 2016 [120] proved that the null hypothesis that the observed interannual variability in the winter WACS pattern might primarily be an expression of atmospheric variability rather than an atmospheric response to sea ice variability can't be rejected. One consistent interpretation of the results is that large-scale atmospheric circulation variability produces southerly wind anomalies that push the Barents Sea ice edge northward, steer warm air into the region, and reduce Barents Sea THF, and that are ultimately associated with cold Siberian temperatures downstream.

Ye and Messori 2020 [141] identified two atmospheric circulation modes over the North Atlantic–northern Eurasian sector that displayed strong positive trends over the same period (1990–2012) and can explain a large part of the observed decadal WACE pattern. Both modes bear a close resemblance to well-known teleconnection patterns and are relatively independent from variability in Arctic sea ice cover. Enhanced intraseasonal activity of the two circulation modes increases blocking frequencies over Greenland, the Ural region, and north Asia, which drive anomalous moisture/heat flux toward the Arctic and alter the downward longwave radiation. This also weakens warm advection and enhances transport of cold Arctic airmasses towards Eurasia.

This review illustrates that the climate of the Arctic is undergoing fast and remarkable changes that produce both local and global significant effects on different areas (natural ecosystems, human communities and global climate); moreover it suggests that warm extremes in the Arctic can have impacts on human activities and the polar environment.

1.3 Arctic warm extremes: state of the art

In Section 1.2 the remarkable importance of the Arctic region in several aspects—from biodiversity to global climate regulation—has been illustrated together with some opportunities (e.g. opening of new shipping routes) and multiple risks (e.g. increase in mid-latitude extreme weather events, drastic changes in marine and terrestrial ecosystems, sea level rising, climate warming positive feedbacks) arising by its strong warming trend. This section presents some results obtained in the recently growing study area of Arctic temperature extremes, concentrating on the hot ones.

The temperature extremes have been linked to a number of drivers, ranging from

perturbations in the tropospheric polar vortex (Moore 2016 [76]) to tropically forced planetary waves (Lee et al. 2011 [62]; Lee 2012 [61]; Flournoy et al. 2016 [35]) and the constructive interference between stationary waves and transient eddies (Baggett and Lee 2015 [5]; Goss et al. 2016 [39]; Baggett et al. 2016 [6]). A common feature of these mechanisms is that they typically lead to a more meridionally oriented circulation, which favors the intrusion of warm and humid air masses from midlatitudes into the high Arctic. A number of recent studies have highlighted that these intrusions result in very discontinuous meridional moisture fluxes into the Arctic region, with a small number of extreme events effectively setting the net seasonal transport value (Woods et al. 2013 [138]; Liu and Barnes 2015 [64]; Dufour et al. 2016 [29]; Naakka et al. 2019 [78]). Such injections induce a transition of the atmosphere from a cold and clear to a warm and opaque state, where the trapping of longwave radiation provides a positive warming feedback with a strong impact on the surface energy balance and sea ice (D.-S. R. Park et al. 2015 [87]; H.-S. Park et al. 2015 [88]; Woods and Caballero 2016 [137]). In addition to air mass injections, near-surface warm temperature anomalies in the Arctic have been linked to anticyclonic flow anomalies (Pfahl and Wernli 2012 [97]; Knudsen et al. 2015 [56]; Ding et al. 2017 [28]; Wernli and Papritz 2018 [135]).

Messori et al. 2018 [73] investigated the salient features and drivers of wintertime (November-February) warm spells in the high Arctic (poleward of 80°N) over the period 1979-2016. They found that warm extremes are characterized by an anomalous SLP (sea level pressure) and geopotential height dipole, with a low over the Canadian and Greenland's Arctic sector and a high over the Eurasian Arctic sector, conducive to meridional advection of heat from the Atlantic sector into the Arctic basin (Figure 1.7). A similar large-scale pattern has been associated with enhanced meridional moisture transport and wintertime sea ice decline over the Barents and Kara Seas (Luo et al. 2017 [65]). Indeed, Messori et al. 2018 [73] showed that winter warm extremes are typically preceded by intense moisture transport episodes into the high latitudes. At synoptic scales, these intrusions are further favored by cyclones that transport moist air masses residing in the Norwegian Sea toward the high Arctic. Cyclones generated in the North Atlantic do not generally penetrate into the Arctic, and the high-latitude cyclones are generated locally [73]. So the atmospheric moisture contained in the moisture intrusion events appears to be relayed into the Arctic via an interaction of several cyclonic systems centered at different latitudes. The moisture intrusions lead to a weakening of the near-surface temperature inversion in the Arctic basin, while their uplift drives positive cloudiness anomalies there.

Studying a prolonged warm period occurred in winter 2016, Kim et al. 2017 [55] concluded that it was triggered by an Atlantic windstorm, which injected considerable amounts of heat and moisture into the Arctic, and sustained by a following prolonged blocking period. In addition, they proved with numerical experiments that warming effect of sea ice loss and associated upward turbulent heat fluxes was relatively minor in the investigated event. This is in accordance with the results of Sorokina et al. 2016 [120] and Cho and

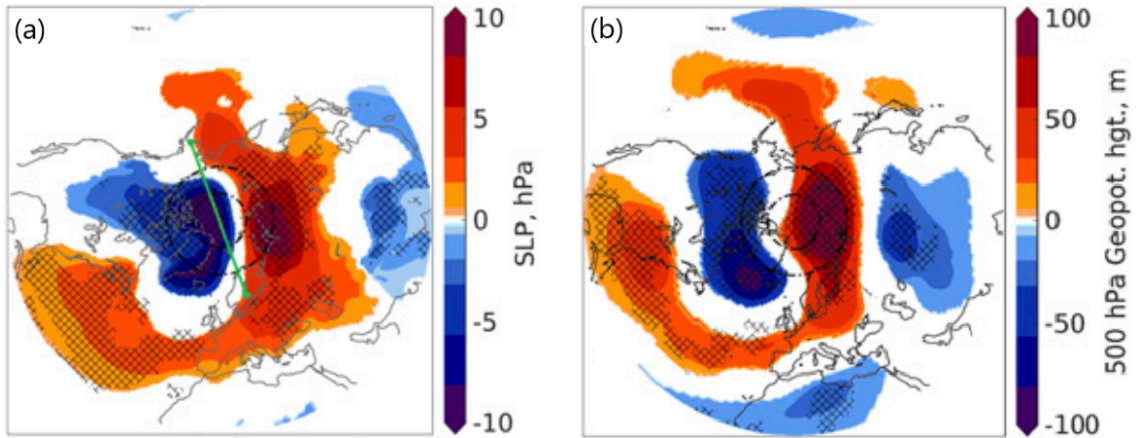


Figure 1.7: Composite SLP (a) and 500-*hPa* geopotential height (b) anomalies for warm extremes at lag 0 days relative to peak temperature anomaly. Only statistically significant anomalies are shown; cross-hatching shows regions of high sign agreement. Taken from Figure 3b and 4b of Messori et al. 2018 [73].

Kim 2020 [20] (see previous Section). But according to Overland, as reported in Simpkins 2017 [118], the absence of sea ice plays a significant role in helping warm air to maintain the heat while crossing open water, allowing its trajectory to reach near to the North Pole.

Using 10-day kinematic backward trajectories, Papritz 2019 [86] investigated the thermodynamic characteristics and evolution of air masses that lead to the formation of extreme warm anomalies (top 5% of all air masses) in the high Arctic ($\geq 80^\circ\text{N}$) lower troposphere (lowermost 100 *hPa*) during winter (DJF) and summer (JJA). Based on a categorization of air masses according to their thermodynamic evolution in $\Delta\theta-\Delta T$ phase space, he quantified the relative importance of transport (e.g. subsidence and poleward transport) and diabatic processes (e.g. surface sensible heat fluxes), as illustrated in Figure 1.8.

Papritz’s principal finding is that subsidence-induced adiabatic warming is by far the most important process for air masses with transport governing the formation of the warm anomaly. This is particularly true in summer, where 70% of all warm extreme air masses are due to subsidence. Most of these air masses originate in the Arctic midtroposphere (Figure 1.9 (b) and (e)), and the subsidence is predominantly driven by anomalous blocking over the Barents, Kara, and Laptev Seas in winter and in the high Arctic in summer.

Another result is that air masses predominantly affected by diabatic heating are a wintertime phenomenon contributing 40% of all air masses in DJF and 10% in JJA. They are related to marine cold air outbreaks in the Barents and Nordic seas, as well as the Labrador Sea (Figure 1.9 (d)) that form as the result of the advection of radiatively

Category	Definition	Key characteristics	Example of characteristic airstream
$\Delta\theta+\Delta T-$	$\Delta T < 0, \Delta\theta > 0$	Diabatically heated, ascending	Warm conveyor belt
$\Delta\theta+\Delta T+$	$\Delta T > 0, \Delta\theta > 0$	Diabatically heated, little vertical motion	Marine cold air outbreak
$\Delta\theta-\Delta T+$	$\Delta T > 0, \Delta\theta < 0$	Diabatically cooled, subsiding	Subsidence in blocking anticyclone
$\Delta\theta-\Delta T-$	$\Delta T < 0, \Delta\theta < 0$	Diabatically cooled, little vertical motion	Poleward-moving warm air mass

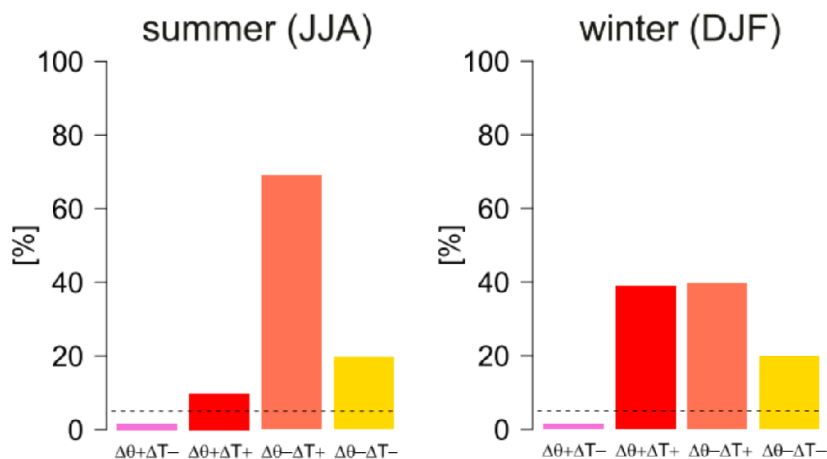


Figure 1.8: Top: definition and key characteristics of trajectory categories. Bottom: fraction of trajectories in each category for (left) summertime and (right) wintertime extreme warm anomalies. The dashed lines indicate 5%. Taken from Papritz 2019 [86].

cooled polar air masses over the relatively warm ocean surface, where they are heated by surface sensible heat fluxes.

Finally, a striking outcome is that lower-tropospheric poleward transport of warm air masses from lower latitudes contributes only about 20% in both seasons. Such transport is favored in winter by a poleward shift of the North Atlantic storm track, whereas the origin of these air masses in summer is largely confined to the Arctic, the Nordic seas and the North Pacific (Figure 1.9 (c)).

Nevertheless, injections of warm and humid air masses are likely of a higher importance for temperature extremes at higher altitude as well as for cloud formation in the Arctic, which directly affects the surface energy balance via their radiative impact (D.-S. R. Park et al. 2015; H.-S. Park et al. 2015; Woods and Caballero 2016). This view is supported by the observation that intense poleward moisture transports do not peak near the surface but further aloft (Laliberté and Kushner 2014; Woods and Caballero 2016; Dufour et al. 2016; Naakka et al. 2019)—a consequence of the isentropic slope at the edge of the polar dome that requires poleward-moving air masses to ascend (Bozem et al. 2019). In addition, injections of air masses with low potential vorticity from lower latitudes into the Arctic upper troposphere play an important role for the amplification of upper-tropospheric ridges and the formation of blocks, which in turn are important drivers of subsidence (Pfahl et al. 2015; Ding et al. 2017; Wernli and Papritz 2018).

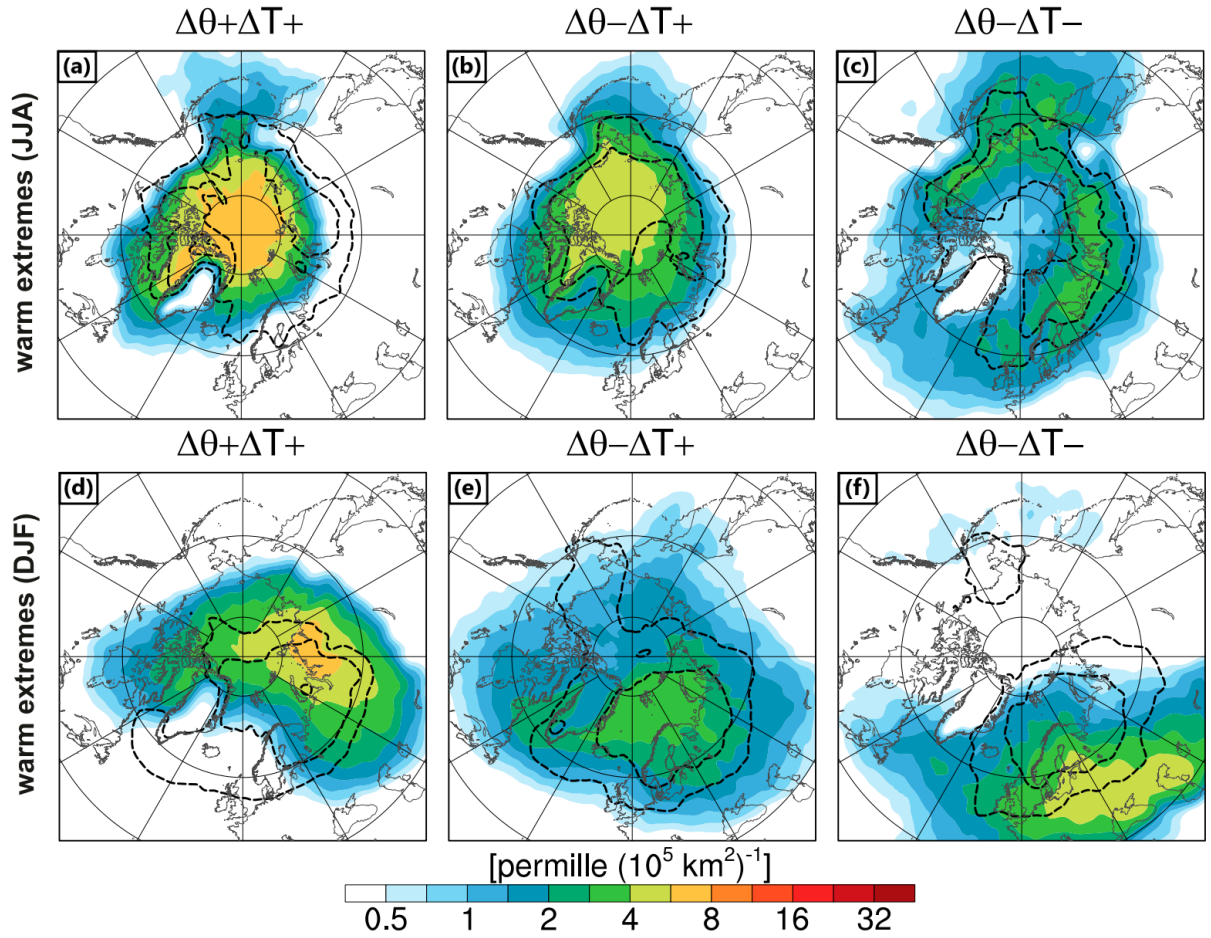


Figure 1.9: Air mass origin maps showing the probability of finding a trajectory of a specific category at a certain location 10 days ($t = -240$ h; shading) and 3 days [$t = -72$ h; dashed; contours at 1, 4, and $16\text{‰}(10^5 \text{ km}^2)^{-1}$] prior to the occurrence of the extreme temperature anomaly for (a)–(c) summertime and (d)–(f) wintertime extreme warm anomalies. Note the logarithmic color scale. Taken from Papritz 2019 [86].

Therefore, as seen thus far, many progresses were made in the last decades in the comprehension of the basic mechanisms that lead to warm extremes in the Arctic region and some light was shed on their complex interplay. But there are many questions still without answer.

1.4 This study

Until now Arctic warm extremes have been studied mostly from an overall point of view, considering their mean characteristics and precursors (e.g. Messori et al. 2018 [73]; Papritz 2019 [86]), or focusing on one specific particularly intense event (e.g. Kim et al. 2017 [55]; Simpkins 2017 [118]). Moreover, the attention was concentrated primarily on winter and secondarily on summer events, almost ignoring the intermediate seasons. The present thesis work aims to distinguish, separately for each of the four seasons, Arctic warm extremes in different classes on the base of the circulation regimes that characterize them on a hemispheric scale (30°-90°N). This analysis is conducted in the perspective of improve Arctic heatwave predictability, due to the relevant local and global impacts of this phenomenon (see Section 1.2).

Chapter 2 provides a definition of Arctic heatwaves, that is still missing, combining the general structure reported in Section 1.1 with the approach designed by Messori et al. 2018 [73]. Furthermore, it explains the hierarchical clustering algorithm used for performing the classification and the methods used to assess the stability of the resulting clusters. The clustering algorithm was imported from Stefanon et al. 2012 [122] but utilized on 500-*hPa* geopotential anomalies instead of surface temperature anomalies (see Section 2.2).

Chapter 3 illustrates the circulation and temperature patterns resulting from the classification, with a particular attention on the winter ones. Moreover, the temporal series of the different heatwave types are examined in order to reveal eventual changes in their frequencies of occurrence during the study period (1979-2019). Finally, heatwave intensities and time lengths are investigated, evidencing differences and analogies between the different clusters and seasons.

In Chapter 4 the results are discussed in the light of the previous studies on the main physical mechanisms causing Arctic warm extremes trying to find eventual correspondence between them and the different clusters. Moreover, some ideas for future studies are proposed.

Chapter 5 summarize the conclusions and suggests further analyses in order to answer the main questions arising from this thesis work.

2 | Data and Methods

The analysis is conducted over the period January 1979 – December 2019 (41 years) and is based on ERA5, the latest atmospheric reanalysis produced by the European Centre for Medium-Range Weather Forecasts (ECMWF). This product outperforms other reanalyses in the tropospheric Arctic region (Hersbach et al. 2020 [47]; Graham et al. 2019 [40]).

Reanalysis combines model data with observations from across the world into a globally complete and consistent dataset. This principle, called data assimilation, is based on the method used by numerical weather prediction centres, where every so many hours (12 hours at ECMWF) a previous forecast is combined with newly available observations in an optimal way to produce a new best estimate of the state of the atmosphere, called analysis, from which an updated, improved forecast is issued [46]. Reanalysis works in the same way, but at reduced resolution to allow for the provision of a dataset spanning back several decades. Moreover, differently from analysis, reanalysis use the same model (not time-varying) over the entire time period, providing a uniform performance.

Ensemble means of geopotential at 500 *hPa* [45] and 2-*m* temperature [46] are used for the entire region north to latitude 30°N; they have a horizontal resolution of $0.5^\circ \times 0.5^\circ$ and a 3-hourly temporal resolution but, in order to reduce the dimension of the datasets, for every grid point only 4 values/day are considered (00:00, 06:00, 12:00, 18:00 UTC), from which daily means are calculated.

2.1 Heatwave definition

The preliminary part of this work is to create a unique definition of Arctic heatwave valid for all seasons. First, the procedure conceived by Messori et al. 2018 [73] and recovered by Papritz 2019 [86], is used. Two-meter temperature anomalies are defined as deviations from a time-varying climatology that is calculated by a combination of a 21-day and a 9-yr running means. Hence, the climatological mean temperature for a given day d of a given year y is the average value of the set of data S_{dy} defined by:

$$S_{dy} = \bigcup_{j=y-4}^{y+4} \bigcup_{i=d-10}^{d+10} T_{j,i}$$

where $T_{j,i}$ is the daily mean temperature value for a day i of year j . For example, the climatological value for 11 January 2004 is the mean of every 1-21 January period between 2000 and 2008. The 21-day running mean ensures a smooth variation of the seasonal cycle and the 9-yr running mean ensures a relatively uniform distribution of extreme events across our analysis period.

The present study aims to identify the large-scale atmospheric circulation drivers of Arctic heatwaves, therefore it has to be able to individuate warm extremes along the entire study period. The definition of climatology adopted here allows to reach this objective. Indeed, if a simple daily climatology were computed over the full dataset (1979-2019), the majority of the heatwaves, especially in winter, would fall in the last decade due to the strong warming trend of the Arctic region, showed in Figure 2.1.

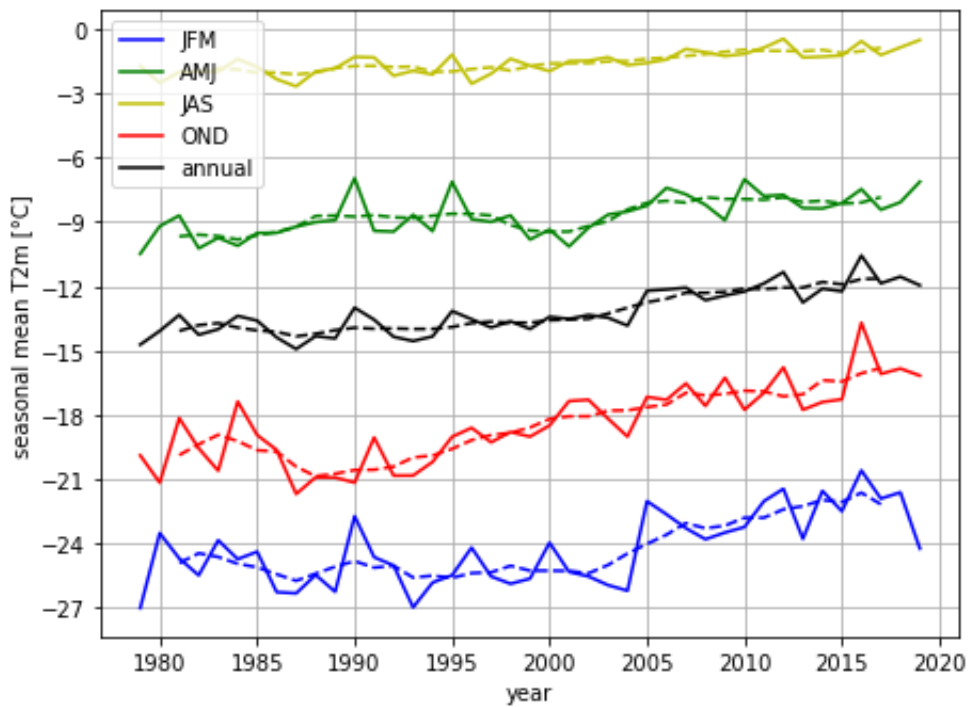


Figure 2.1: Temporal evolution of the seasonal mean 2- m temperature ($^{\circ}\text{C}$) over the $75\text{-}90^{\circ}\text{N}$ Arctic domain (solid line) and the corresponding 5-yr running mean (dashed line) for the four seasons (winter-blue, spring-green, summer-yellow, autumn-red). In black the annual mean.

At the beginning and end of the time series it is impossible to apply the above-mentioned definition of climatology. Therefore, if n is one of the first five years of the dataset ($n=1979,\dots,1983$) then for the first ten days of n (1-10 January) the running mean is computed from 1980 to $n+4$ and for the remaining days of n (11 January-31 December) the running mean is computed from 1979 to $n+4$. Similarly, if m is one of the last

five years of the dataset ($m=2015,\dots,2019$) then for the the last ten days of m (22-31 December) the running mean is computed from $m - 4$ to 2018 and for the remaining days of m (1 January-21 December) the running mean is computed from $m - 4$ to 2019. Then, a single temperature anomaly value per day is obtained making an area-weighted average of temperature anomalies over the Arctic domain (in the present study considered from $75^\circ N$ to the North Pole, as illustrated at the end of this Section).

As regard the persistence and amplitude requirements, Messori et al. 2018 [73] performed a 5-day running mean to the anomaly time series and then selected the 50 warmest events.

Instead, here the general structure of heatwave definitions, already examined in Section 1.1), is used. In particular, seasonal $90^{th}pct$ of the anomalies are computed over the full dataset (1979-2019). In the present study the seasons' division is:

- winter = January-February-March (JFM)
- spring = April-May-June (AMJ)
- summer = July-August-September (JAS)
- autumn = October-November-December (OND)

A day in which the temperature anomaly is higher then its seasonal $90^{th}pct$ is defined *Arctic hot day* (AHD or more briefly HD). An *Arctic heatwave* (AHW or more briefly HW) is defined as a period of at least 3 consecutive HDs.

Preliminary tests using seasonal 95^{th} percentiles did not evidence qualitative differences in the seasonal mean heatwave temperature and geopotential maps compared to those obtained with 90^{th} percentiles. $90^{th}pct$ was preferred in order to have enough events to perform seasonal analyses with a 41-yr dataset.

The *intensity* of an HW is defined as the mean temperature anomaly of the HDs that compose the HW. The *magnitude* of an HW is defined as the product of its intensity and its duration. This definition of magnitude is a simpler version of the definition designed by Russo et al. 2015 [108] (see Section 1.1).

Messori et al. 2018 [73] and Papritz 2019 [86] focused on the high Arctic choosing as domain the region poleward of $80^\circ N$. In the present work it is preferred to consider a larger portion of the Arctic, specifically the Arctic domain is defined as the region poleward of $75^\circ N$ allowing to embrace a large fraction of the Arctic Ocean while still excluding the majority of the landmass that surround it.

The decision of not extending further the Arctic domain is motivated by the fact that if a broader domain is selected then the temperature variability over subpolar land-covered regions would play a dominant role in determining heatwaves due to their stronger climate variability.

This can be seen in Figure 2.2 in which two cases are compared: the HW definition over

the 75-90°N domain, used in this study, and the HW definition over the 60-90°N domain (i.e. considering the area-weighted average of temperature anomalies over the region poleward of 60°N). Each panel is obtained averaging all days belonging to heatwaves, these latter identified by the corresponding HW definition: over 60-90°N in panels (a), (c); over 75-90°N in panels (b), (d).

Panel (a) shows that if the Arctic domain is extended down to 60°N mean anomalies above 2.8 K occur mostly over continental landmasses and exceed 4.2 K almost exclusively over northern Siberia. On the contrary the Atlantic sector of the high Arctic does not reach positive anomalies above 1.4 K.

The situation is reverse limiting the domain to 75°N, in which case the highest mean temperature anomalies are found in the Atlantic-Eurasian sector of the high Arctic, as shown in panel (b).

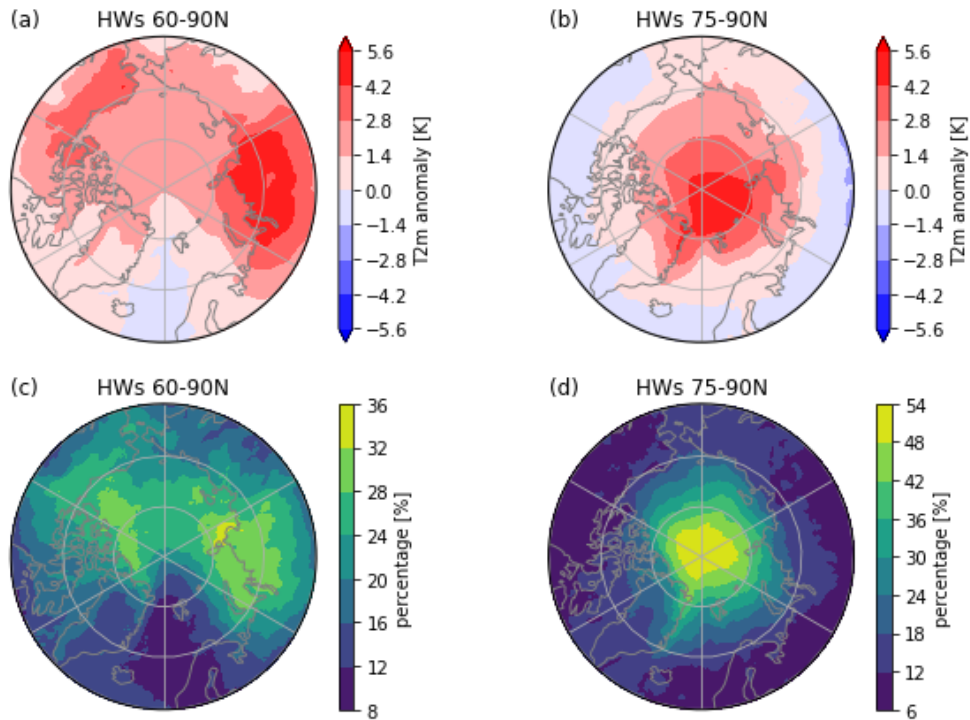


Figure 2.2: Mean 2-*m* temperature anomalies in shadings (in *K*) for all days belonging to heatwaves defined on the domain 60-90°N (a) and on the domain 75-90°N (b). Percentage of all days belonging to heatwaves, defined on the domain 60-90°N (c) and on the domain 75-90°N (d), that are grid point-hot days.

If every single day belonging to any heatwave is called HW-day then panels (c) and (d) illustrate for every grid-point the percentage of HW-days that are grid point-hot days (i.e. days with grid-point temperature anomaly above its seasonal 90th percentile). These

two panels confirm that using the Arctic domain chosen in this work (d), instead of the broader one that spans from the North Pole to 60°N (c), brings to a selection of events more North Pole centered.

According to the heatwave definition illustrated in this Section, 180 heatwaves are identified in the study period (1979-2019). They contain 86.66% of the total number HDs and have a mean duration of 7.2 days.

2.2 Clustering algorithm

From the procedure exposed in section 2.1 180 Arctic heatwaves are obtained over the 41-yr period 1979-2019. For the purpose of highlighting seasonal differences the 180 HWs are divided into 4 groups according to the seasons of belonging. Each heatwave that is at the turn of two seasons is assigned to the season that includes the majority of the hot days of the heatwave.

For every heatwave all daily temperature anomaly maps belonging to it are averaged producing its ‘event map’. The same is done for 500-*hPa* geopotential height anomaly, calculated with the same procedure used for the temperature anomaly (described in section 2.1), i.e. subtracting a time-dependent climatology obtained by combining of a 21-day and a 9-yr running means. The anomaly correlation coefficient r , called also cosine similarity, between two event maps \mathbf{p} and \mathbf{q} is defined as:

$$r(\mathbf{p}, \mathbf{q}) = \frac{\sum_{i=1}^N \sum_{j=1}^M p_{ij} q_{ij}}{(\sum_{i=1}^N \sum_{j=1}^M p_{ij}^2)^{1/2} (\sum_{i=1}^N \sum_{j=1}^M q_{ij}^2)^{1/2}}$$

where \mathbf{p} and \mathbf{q} refer to the maps which are matrices of size M by N along the longitudinal and latitudinal axes respectively. The quantities p_{ij} and q_{ij} are the values of \mathbf{p} and \mathbf{q} at coordinates (i, j) along the longitudinal and latitudinal axes, respectively.

Stephanon et al. 2012 [122] implemented a method for classifying heatwave events in the Euro-Mediterranean region on the base of the spatial configuration of temperature anomalies. Here, that method is applied to 500-*hPa* geopotential height anomalies in order to classify Arctic heatwaves events on the base of their large-scale atmospheric circulation drivers.

According to this, on the extended region that ranges from North Pole down to 30°N, an agglomerative hierarchical clustering algorithm is applied, once for each season, to the geopotential height anomaly event maps belonging to the same season.

The general structure of an agglomerative hierarchical clustering algorithm is the following:

1. at the initial step, each data point (i.e. each event map) forms a cluster;
2. the two ‘nearest’ clusters are then merged by pair into a new cluster, with the distance between two clusters measured using a metric;

3. point 2 is iterated until a stop criterion is met, which sets the number of clusters.

The qualifier ‘agglomerative’ indicates that the algorithm proceeds by progressively merging clusters, starting from the single data points (bottom-up approach). ‘Hierarchical’ denotes that at every time step corresponds a set of clusters and hence the whole of the sets forms a hierarchy of clusters. One reason for the decision of using hierarchical clustering was the fact that no a priori information about the number of clusters is required.

All clustering methods require a metric definition d . Here, we use the same pseudometric used by Stephanon et al. 2012 [122], based on the anomaly correlation coefficient r . First, we define a distance d' between any two maps \mathbf{p} and \mathbf{q} as:

$$d'(\mathbf{p}, \mathbf{q}) = 1 - r(\mathbf{p}, \mathbf{q})$$

where $r(\mathbf{p}, \mathbf{q})$ is the anomaly correlation coefficient between \mathbf{p} and \mathbf{q} . The distance between two clusters C_1 and C_2 is then computed as the distance between their two farthest members, in other terms:

$$d(C_1, C_2) = \max(d'(\mathbf{p}, \mathbf{q})) \quad \text{for all } \mathbf{p} \in C_1, \mathbf{q} \in C_2$$

This definition of distance is chosen because is particularly suited to distinguish between different spatial patterns, while it is less sensitive to the amplitude of the anomalies [122]. Note that $0 \leq d \leq 2$. $d = 1$ corresponds to orthogonal vectors, $d = 0$ is for parallel vectors with a positive coefficient and $d \geq 1$ when vectors are anti-correlated.

It is important to report that an alternative classification was performed with Ward hierarchical clustering method (already used by Cheng and Wallace 1993 [18]), which employs a Euclidean metric, and it does not showed significant qualitative differences in the results.

In order to select the optimal number of clusters n_{op} a *dissimilarity index* $d_I(n)$, function of the number of clusters n , is defined as the minimum inter-cluster distance (i.e. the distance of the two closest clusters). n_{op} is determined by the number of clusters n , with $2 \leq n \leq 6$, for which the difference $\Delta d_I(n) = d_I(n) - d_I(n + 1)$ is maximum. Given that passing from n to $n+1$ means that one of the n clusters is split into two clusters, a small difference $\Delta d_I(n)$ means that these latter two clusters remain very similar or, in other terms, this partition do not provide different patterns but merely place random borders within similar patterns [122]. So it is crucial not to choose an n_{op} too high. On the contrary it is important not to merge clusters that have appreciable differences. The criterion chosen here is designed to find a good balance between this two needs.

The seasonal optimal numbers of clusters obtained in this way are: $n_{op}^{JFM} = 3$, $n_{op}^{AMJ} = 2$, $n_{op}^{JAS} = 2$ and $n_{op}^{OND} = 4$ (Figure 2.3). A cluster map is simply defined as the mean of all the event maps that compose the cluster. Cluster maps for the various seasons are illustrated in Chapter 3.

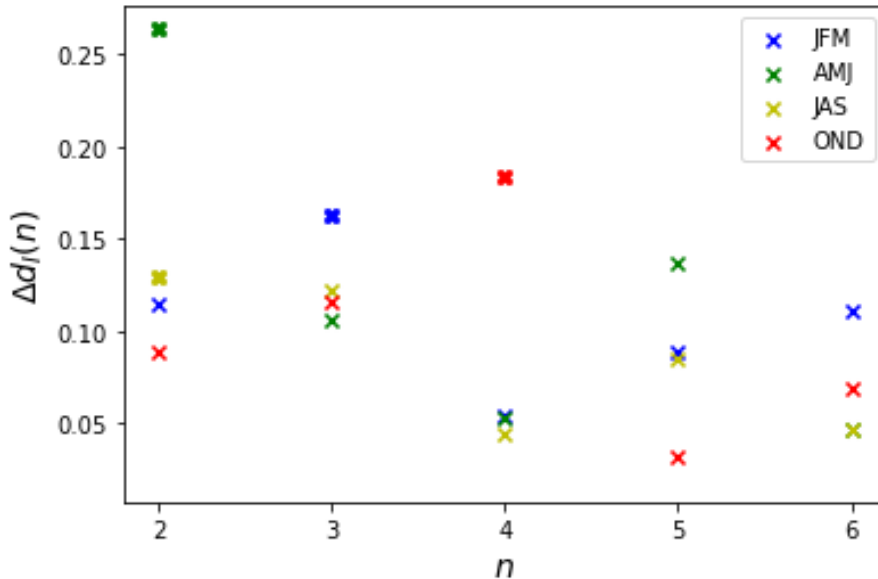


Figure 2.3: Δd_I for the four seasons, varying the number of clusters n . Bold crosses indicates the four maxima that determine the optimal number of clusters n_{op} .

2.3 Cross validation procedure

Following the procedure of Stephanon et al. 2012 [122] a cross validation procedure is used to check the stability of our classification. For every season the 41 year of the dataset are divided in six non-overlapping verification periods (vp), shown in Table 2.1. The division was initially done in the same way for all seasons: five 7-yr period and one 6-yr period. But finally this division was modified for autumn and winter in order to reduce the range of variation of the number of events among the different verification periods, obtaining a better sampling. One time for each verification period, the current vp is eliminated from the dataset and the clustering is performed on the remaining years (reduced period) until the n_{op} of the full period is reached. Next the n_{op} clusters of the reduced period are associated to the n_{op} clusters of the full period through a one-to-one mapping. The selected mapping from all the possible one-to-one mapping is that for which the sum of the n_{op} anomaly correlation coefficient relative to the n_{op} clusters' couples ($\sum_{i=0}^{n_{op}} r$) is maximum. Heatwaves from the verification period are then associated to the clusters of the reduced period, according to the nearest distance (still using the metric employed in the clustering algorithm). We compare the membership of the verification period episodes to the reduced period clusters with the membership to the full period clusters, according to the selected mapping. Once this procedure is repeated six times for the six verification periods and corresponding reduced periods, for each cluster the number n_c of verification period heat waves that are correctly attributed are calculated.

These results are compared to a Monte Carlo test. The Monte Carlo test is constructed by proceeding as above, except that heatwaves from the verification period are associated to the reduced period clusters in a purely random way, and the procedure is repeated 10^5 times. A histogram is constructed with the 10^5 values of n_c , that are indicated as n_c^{mc} . Significance is here defined as the percentage of n_c^{mc} that are lower than n_c . For example in Figure 2.4, that shows the result of the Monte Carlo test for one of the summer cluster (named JAS1) whose n_c is 11, the significance is the percentage of the total area that is yellow coloured (in that case 89.5%).

JFM	years	n° of events	AMJ	years	n° of events
vp1	1979-1985 (7)	7	vp1	1979-1985 (7)	6
vp2	1986-1992 (7)	10	vp2	1986-1992 (7)	9
vp3	1993-2000 (8)	10	vp3	1993-1999 (7)	7
vp4	2001-2006 (6)	9	vp4	2000-2006 (7)	9
vp5	2007-2013 (7)	6	vp5	2007-2013 (7)	8
vp6	2014-2019 (6)	9	vp6	2014-2019 (6)	7

JAS	years	n° of events	OND	years	n° of events
vp1	1979-1985 (7)	5	vp1	1979-1984 (6)	9
vp2	1986-1992 (7)	5	vp2	1985-1990 (6)	7
vp3	1993-1999 (7)	9	vp3	1991-1997 (7)	7
vp4	2000-2006 (7)	6	vp4	1998-2004 (7)	8
vp5	2007-2013 (7)	9	vp5	2005-2012 (8)	6
vp6	2014-2019 (6)	6	vp6	2013-2019 (7)	6

Table 2.1: Verification periods used in the clustering cross validation procedure for the four seasons (JFM, AMJ, JAS, OND). The numbers in parenthesis are the length of the verification periods in years.

The aforesaid definition of significance, imported from Stephanon et al. 2012 [122], is based on the random assignment of the verification period HWs, i.e. on the null hypothesis that they cannot be classified in the clusters obtained from the reduced period. This is a valid but partial approach. So in this work another independent and complementary way to assess the stability of a cluster is designed: r_m . It is the mean of the six anomaly correlation coefficient r between the full period cluster map and the six reduced period cluster maps. r_m gives a simple, intuitive measure of the resistance of the cluster pattern to changes induced by the cross validation procedure.

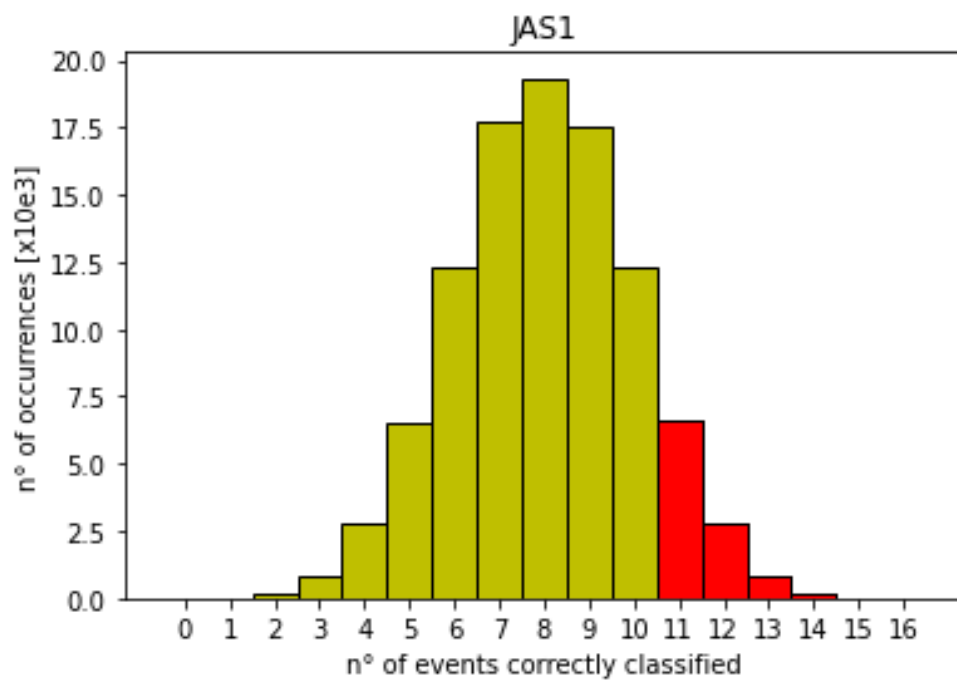


Figure 2.4: Histogram resulting from the monte carlo test for the cluster JAS1. Red columns are those corresponding to a number of correctly classified events equal to or greater than the number of events correctly classified in the cross validation procedure (in this case 11).

3 | Results

In this Chapter the results of the clustering procedure are illustrated. Section 3.1 focuses on the winter season, whereas Section 3.2 treats the other ones. Finally, Section 3.3 shows an overview on heatwave duration and intensity among the different seasons and clusters.

3.1 Winter heatwaves

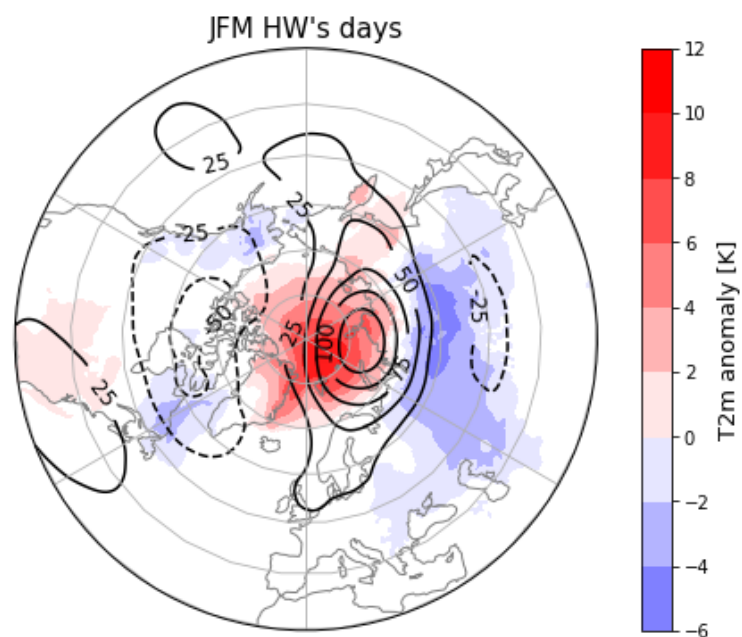


Figure 3.1: Mean 2- m temperature anomalies in shadings (in K) and mean 500- hPa geopotential height anomaly in contours (drawn every 25 m , with zero-line omitted) of all days belonging to winter (JFM) heatwaves. White areas have temperature anomalies between -1 and $1 K$.

Figure 3.1 shows the mean circulation and 2- m temperature anomaly patterns of all days belonging to winter (JFM) heatwaves on a hemispheric scale (30° - 90° N). The 500- hPa geopotential height anomaly manifests a wave number 1 configuration with a marked elongated (from northern Europe to the Pacific Ocean) dipole in the Arctic region formed by an intense anticyclonic anomaly, centered approximately over the Kara sea (where it exceeds 125 m), and a cyclonic less intense pole, situated in the Canadian Arctic (that does not fall below $-60 m$). This features indicate a remarkable alteration of the atmospheric currents in the Arctic that provokes strong southerly flow across Barents, Norwegian and Greenland Seas from the Atlantic and Eurasian regions to the high Arctic. This average anomaly circulation pattern is a characteristic of winter warm extremes that was already found by Messori et al. 2018 [73] (Figure 1.7 (b)) and Papritz 2019 [86] despite the use of slightly different methodologies, of different datasets, of a more restricted Arctic domain ($> 80^{\circ}$ N) and of different winter periods (NDJFM in Messori et al. 2018 [73] and DJF in Papritz 2019 [86]).

Another distinctive trait evident in Figure 3.1 that was already revealed and studied by a multitude of scientific works (see Section 1.2 and references therein) is a marked warm Eurasia-cold Arctic (WACE) pattern. In particular the 2- m temperature anomaly exceeds 8 K in the Eurasian sector of the Arctic north to 80° N and is below $-2 K$ over a vast area that spans from the Caspian Sea to Eastern Siberia, reaching $-5 K$ in central Siberia.

The cluster analysis conducted in the present study aims at identifying different circulation regimes that compose this pattern. The result is shown in Figure 3.2, in which the three winter clusters are displayed.

Heatwaves belonging to cluster (a) feature a pronounced anticyclonic anomaly over Laptev and Kara Seas, conducive for flow from Siberia to the high Arctic through the Barents Sea. In view of this, their pattern is called hereafter Siberian Anticyclonic or simply SA. SA accounts for about half of the winter events (26/51) and has the highest mean duration (7.2 days). It also has the highest mean intensity (4.54 K), even if this can be partially due to the fact that its warm anomaly is more North Pole-centered than for the other two clusters (in Section 2.1 the intensity of a heatwave was defined as its mean temperature anomaly averaged over the domain 75 - 90° N). Moreover SA shows a large cyclonic anomaly over Canada and north Atlantic that peaks over the Irminger Sea, which according to Papritz 2019 [86] is the region with higher intensification of cyclonic activity during Arctic winter warm extremes. Therefore it is likely that this negative pole is explained also by synoptic scale processes.

Cluster (b) is formed by 18 events with a mean duration of 5.8 days. It is referred as Eurasian Anticyclonic, or simply EA, since is countersigned by a marked anticyclonic anomaly over the Eurasian sector of the Arctic, centered over the Barents and Kara Seas and stretched down to the North Atlantic. This configuration favours warm moist advection from the Atlantic to the high Arctic. EA shows also an extensive cyclonic

anomaly, peaked over the Beaufort and Chukchy Seas.

SA and EA together account for the majority of winter events. They both show a geopotential dipole configuration with a marked high latitude anticyclonic pole. Despite their reciprocal similarities, SA and EA are both stable and homogeneous clusters, as attested by the high values of significance and r_m showed in Table 3.1 (see Section 2.3 for their definitions). Furthermore, they both present a WACE pattern, more pronounced in EA in which the cold anomaly, besides central Siberia, extends also over all the European Russia where falls below $-5 K$.

Finally, an interesting difference between SA and EA is that the latter presents a positive temperature anomaly over North America (that exceeds $3 K$ in south-central Canada), whereas the former presents a slight negative temperature anomaly over Canada and Alaska.

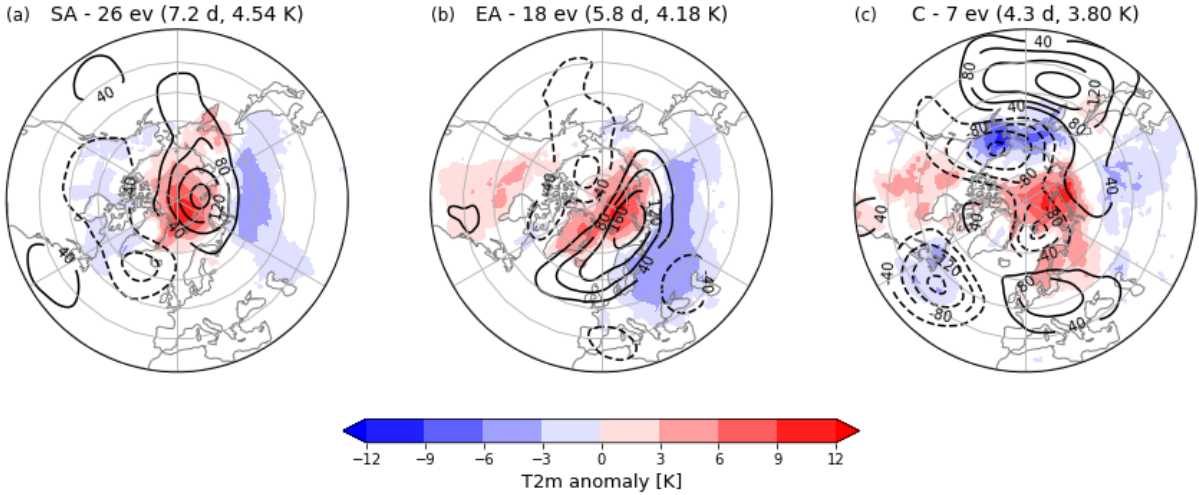


Figure 3.2: Composites of mean 2- m temperature anomalies in shadings (in K) and mean 500- hPa geopotential height anomaly in contours (drawn every 40 m , with zero-line omitted) for the winter clusters. White areas have temperature anomalies between -1.5 and $1.5 K$. Next to the cluster's label the number of events forming the cluster is shown, followed by the mean duration (in days) and the mean intensity (in K) in parenthesis.

	significance	r_m
SA	99.0 %	0.97
EA	99.6 %	0.91
C	99.3 %	0.69

Table 3.1: Significance and mean correlation coefficient (r_m) for winter clusters.

Cluster (c) is noticeable for the absence of an anticyclonic anomaly in polar and subpolar regions. Instead it shows two marked negative geopotential height anomalies, one over the Svalbard and one over northern Alaska. For this reason this cluster is called Cyclonic (C). It is the shorter and less intense winter cluster and contains only 7 heatwaves. The warm anomaly is distinctly shifted toward the Eurasian sector of the Arctic (peaking across Franz Josef Land, Severnaya Zemlya and the Taymyr peninsula with values between 8 and 13 K) and extends down to Scandinavia (entirely above of 3 K). Positive temperature anomalies are found also over central Canada and the central-northern USA. Cold anomalies are particularly pronounced over the eastern-most part of Siberia and over Alaska (in this latter falling below $-9 K$), but are present also over central-eastern Asia (southern Siberia, Mongolia, northern China) and western Atlantic (Newfoundland).

As SA and EA, also C has a high significance but presents a relatively low r_m (Table 3.1), that can only partially be due to its small cardinality and therefore may indicate a quite heterogeneous composition. For this reason, and for its complex configuration, it is interesting to inspect the 7 events that compose it. Figure 3.3 confirms a considerable internal variability in cluster C. It seems to gather those events that do not fit in the other two clusters. Except the short time length, there isn't a marked feature common to all 7 events. But five of them are characterized by the opposition of an anticyclonic anomaly over Europe and a cyclonic anomaly over North Atlantic (a) (b) (f) or over the high Arctic (c) (g).

It is interesting to inspect the time series of the different heatwave types for seeing whether any periodicities or occurrence changes are evident during the study period (1979-2019). Figure 3.4 illustrates how the first decade of the study period was dominated by EA events, whereas the subsequent 10-15 years were characterized by SA heatwaves. The final part of the time series shows a more balanced occurrence of the three heatwaves types.

This temporal evolution is confirmed by Figure 3.5 in which the mean heatwave patterns of the first two decades manifest an evident correspondence with cluster EA and SA, respectively.

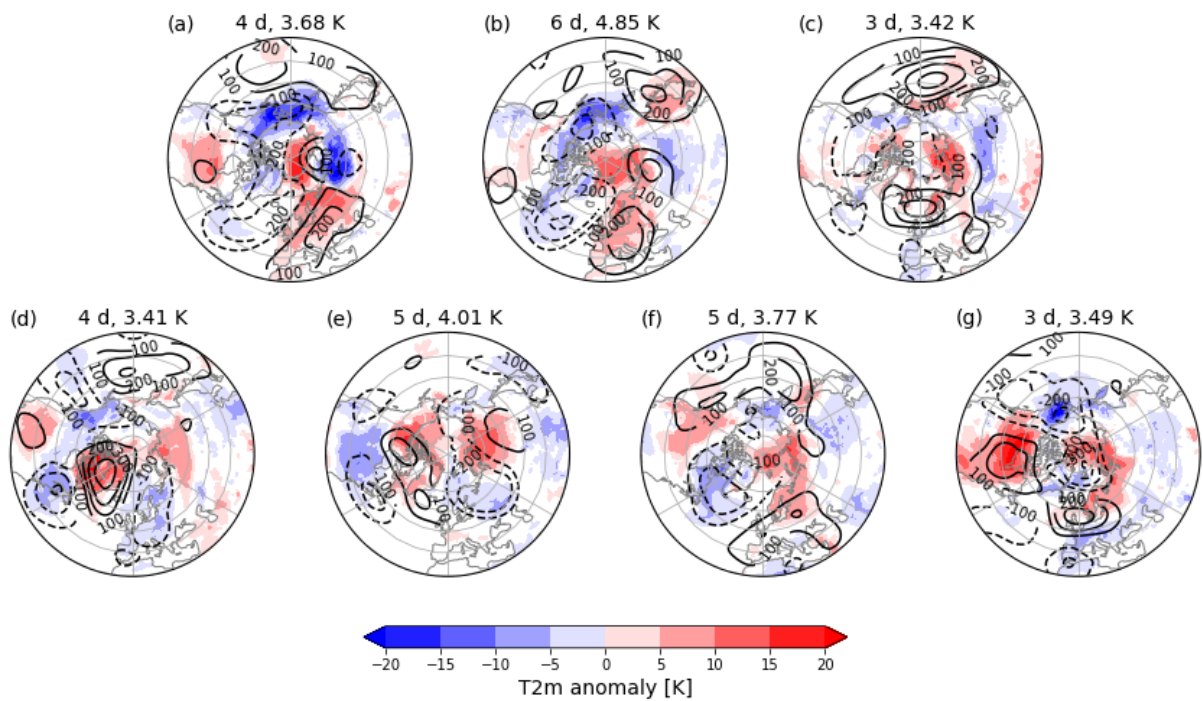


Figure 3.3: Mean 2- m temperature anomalies in shadings (in K) and mean 500- hPa geopotential height anomaly in contours (drawn every 100 m , with zero-line omitted) of the 7 heatwaves belonging to cluster C. White areas have temperature anomalies between -2.5 and 2.5 K . Above each map the corresponding duration (in days) and intensity (in K) are reported.

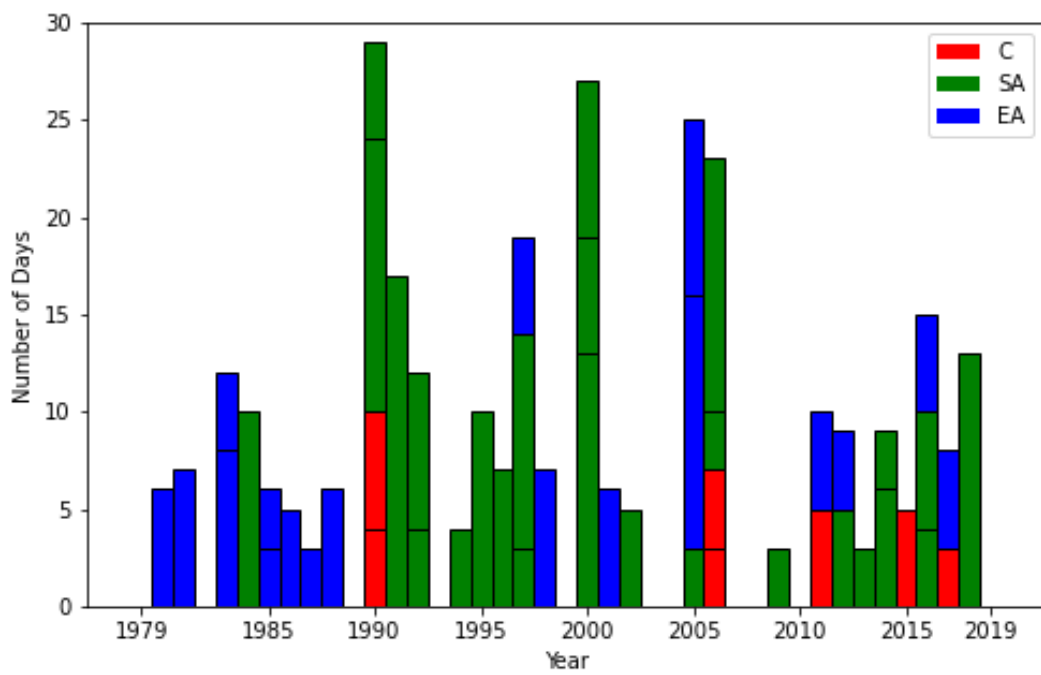


Figure 3.4: Winter Arctic heatwave climatology between 1979 and 2019 with attribution to the three clusters (C, SA, EA). The horizontal black segments separate single events.

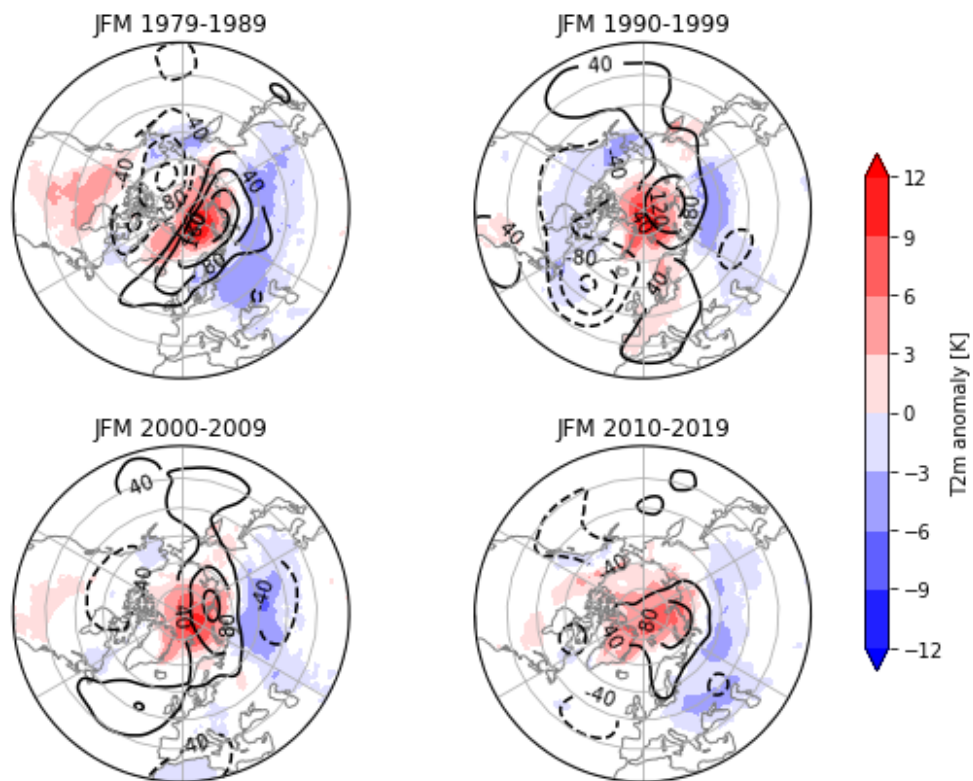


Figure 3.5: Composites of mean 2- m temperature anomalies in shadings (in K) and mean 500- hPa geopotential height anomaly in contours (drawn every 40 m , with zero-line omitted) for winter heatwaves belonging to four subsequent decadal periods: 1979-1989, 1990-1999, 2000-2009 and 2010-2019. White areas have temperatures between -1.5 and 1.5 K .

3.2 Spring, Summer and Autumn heatwaves

The two spring clusters, denoted by the labels AMJ1 and AMJ2, are shown in Figure 3.6. AMJ1 is characterized by a geopotential dipole over the Atlantic sector of the Arctic, with a markedly elongated positive pole that peaks in the North Sea and a more pronounced negative pole that peaks between Greenland and Canada. The highest positive temperature anomalies are found in the Eurasian sector of the Arctic (reaching 6 K), whereas negative temperature anomalies are found in northern Canada (not falling below -4.5 K).

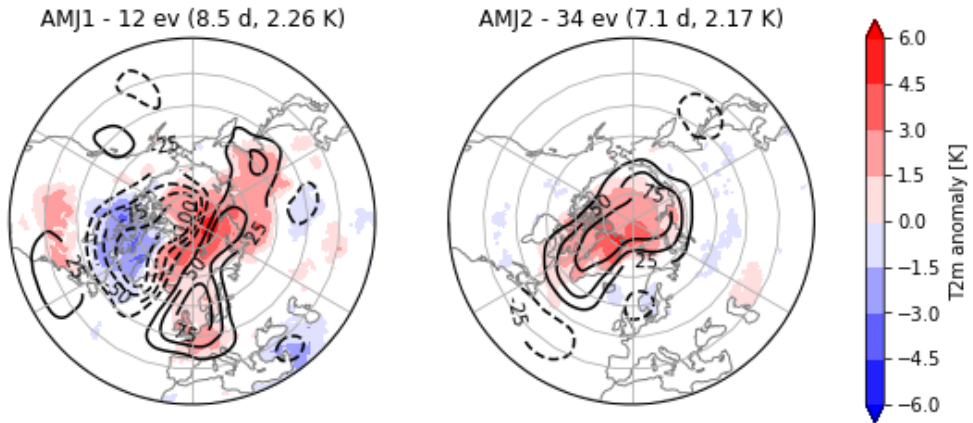


Figure 3.6: As in Figure 3.2 but for spring clusters. Mean 500- hPa geopotential height anomaly contours are drawn every 25 m . White areas have temperatures between -0.75 and 0.75 K.

	significance	r_m
AMJ1	99.7 %	0.87
AMJ2	100 %	0.97

Table 3.2: Significance and mean correlation coefficient (r_m) for spring clusters.

AMJ2 has nearly three times the number of events of AMJ1 and is dominated by a large monopole over the Arctic, stretched towards the Labrador Sea, that coincides with the warm anomalies, which reach its maximum in the north of Greenland (5 K). Pronounced cold anomalies are not present in AMJ2.

The two clusters have similar intensity, but AMJ1 events last averagely 1.4 days more than AMJ2.

Both clusters have high values of significance and r_m certifying their elevated stability (Table 3.2).

The two summer clusters, denoted by the labels JAS1 and JAS2, are shown in Figure 3.7. JAS1 is composed by 16 events with a mean duration of nearly 6 days and presents a cyclonic anomaly that extends from the high Arctic to north-eastern Europe. Around this latter there are three anticyclonic anomalies respectively over the Beaufort Sea, western Siberia and north-eastern Atlantic (which is the most pronounced one). The positive temperature anomaly peaks over northern Greenland (reaching 3.2 K) and the only Arctic sector that does not experience warming is the European one. An extended warm anomalies above 1 K is present over western Siberia and the Turan Depression, whereas a cold one below -1 K is present over Scandinavia and central Europe. JAS1 has a high r_m , but a quite low significance (Table 3.3). Overall JAS1 can be considered moderately stable.

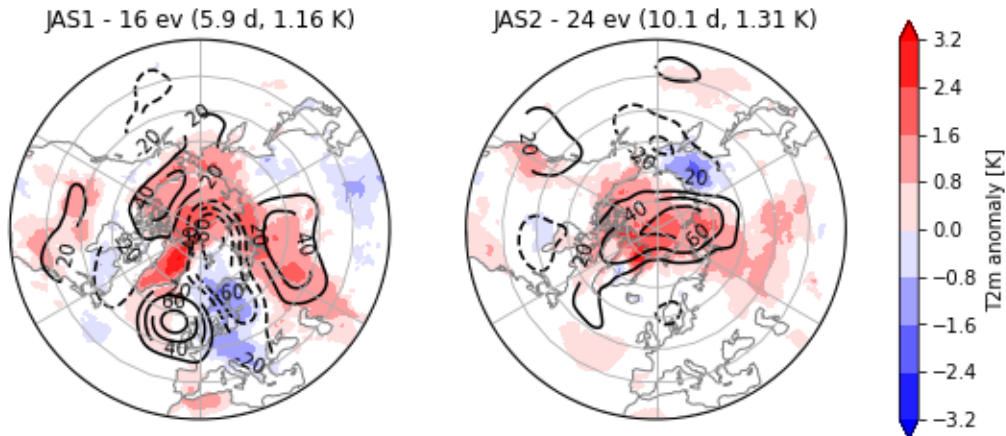


Figure 3.7: As in Figure 3.2 but for summer clusters. Mean 500- hPa geopotential height anomaly contours are drawn every 20 m . White areas have temperature anomalies between -0.4 and 0.4 K.

	significance	r_m
JAS1	89.5 %	0.92
JAS2	99.6 %	0.95

Table 3.3: Significance and mean correlation coefficient (r_m) for summer clusters.

JAS2 is formed by 24 events with a remarkable mean duration of about 10 days and is characterized by an extended positive geopotential height anomaly over the Arctic that peaks between the North Pole and the Taymyr Peninsula, and stretches towards

the Labrador Sea. A cyclonic anomaly is present over the Bering Sea and the extreme north-eastern Russia. The warm anomaly peaks in the high Arctic, reaching its maximum over Ellesmere Island and northern Greenland (nearly 3 K). The only appreciable cold anomaly is in eastern Siberia (however not below -2.2 K).

JAS2 is a stable pattern as proven by high values of both significance and r_m (Table 3.3).

The four autumn clusters, denoted by the labels OND1, OND2, OND3 and OND4, are shown in Figure 3.8.

OND1 is formed by only 3 heatwaves, all of them with the minimum duration accepted by the heatwave definition (3 days). Therefore it represents very rare events, characterized by an anticyclonic anomaly over the Canadian Arctic and a cyclonic one over north-eastern Europe. The warm anomaly is concentrated over the Canadian Arctic Archipelago where values are higher than 8 K . On the contrary the section of the 60°N -zonal band that goes from Scandinavia to the Siberian Pacific coast experience negative temperature anomalies below -5 K .

OND2 is the most numerous (16 events) autumn cluster. It is countersigned by a large positive geopotential height anomaly over the Arctic, slightly shifted towards central-western Siberia, surrounded by three less marked negative anomalies over the north-western Pacific, central-northern Asia and northern Canada. The warm anomaly is spread over the majority of the Arctic Ocean and exceed 5 K in the high Arctic and in north-eastern Siberia.

OND3 is formed by 12 heatwaves with a short mean lifetime (4.5 days). It shows a wave-like geopotential height structure formed by a pronounced negative anomaly centered approximately over south Greenland followed by a positive anomaly over northern Europe and a negative less marked one over western Siberia. The warm anomaly is concentrated over the high Arctic, peaking between the North Pole and the Svalbard ($7.5\text{-}10\text{ K}$).

Both OND2 and OND3 show a pronounced WACE (warm Arctic - cold Eurasia) pattern with anomalies below -5 K over vast areas in central and western Siberia. Table 3.4 attests the elevated stability of clusters OND1 and OND2. OND3 results slightly less robust.

But the only cluster that can not be considered stable is OND4 given that has a low significance and a moderate r_m (Table 3.4). Nevertheless the inspection of the 12 events that compose it shows that two third of them exhibit the threepolar structure emerging from the clustering: a cyclonic anomaly over the north-eastern Atlantic and two anticyclonic anomalies respectively over western Siberia and the Bering Strait. Almost all the Arctic Ocean exhibit positive temperature anomalies but the stronger warming is observed over the Kara Sea and the Taymyr peninsula, and over the Chukchi Sea and extreme north-eastern Siberia.

Both OND2 and OND4 exceed the 8-days mean duration.

Figure 3.9 do not reveal particular periodicities or changes in the occurrences of the different heatwave types during the period for the three seasons illustrated in this Section.

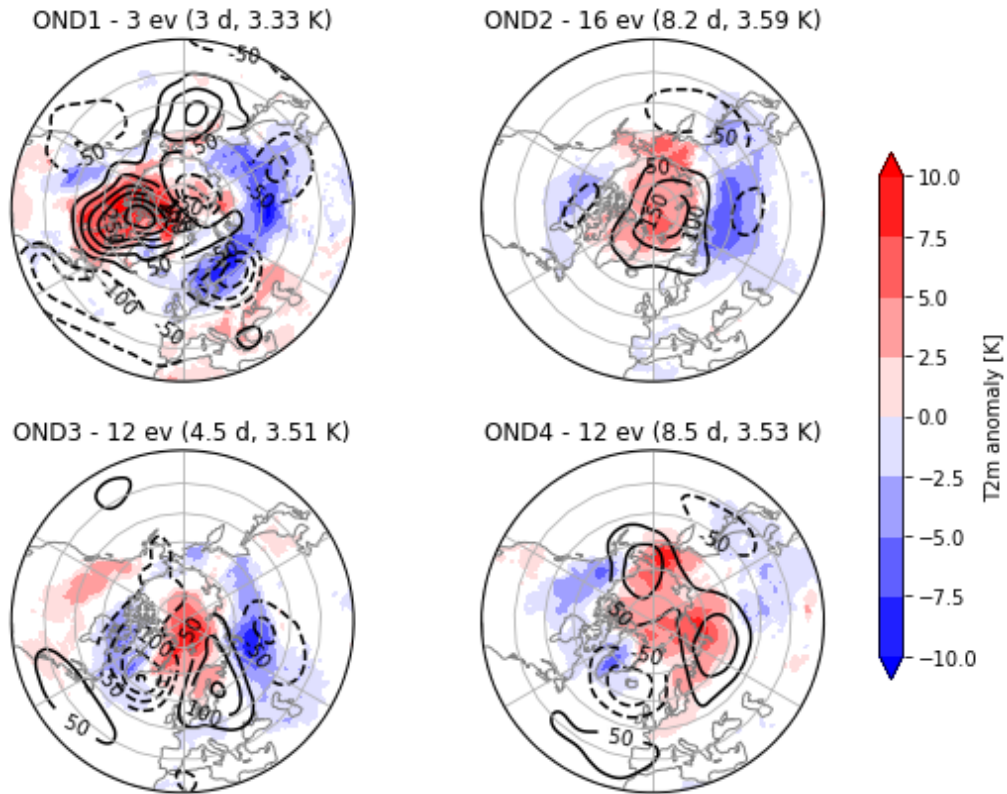


Figure 3.8: As in Figure 3.2 but for autumn clusters. Mean 500- hPa geopotential height anomaly contours are drawn every 50 m . White areas have temperature anomalies between -1.25 and 1.25 K .

	significance	r_m
OND1	98.4 %	0.89
OND2	97.2 %	0.92
OND3	94.7 %	0.87
OND4	84.1 %	0.82

Table 3.4: Significance and mean correlation coefficient (r_m) for autumn clusters.

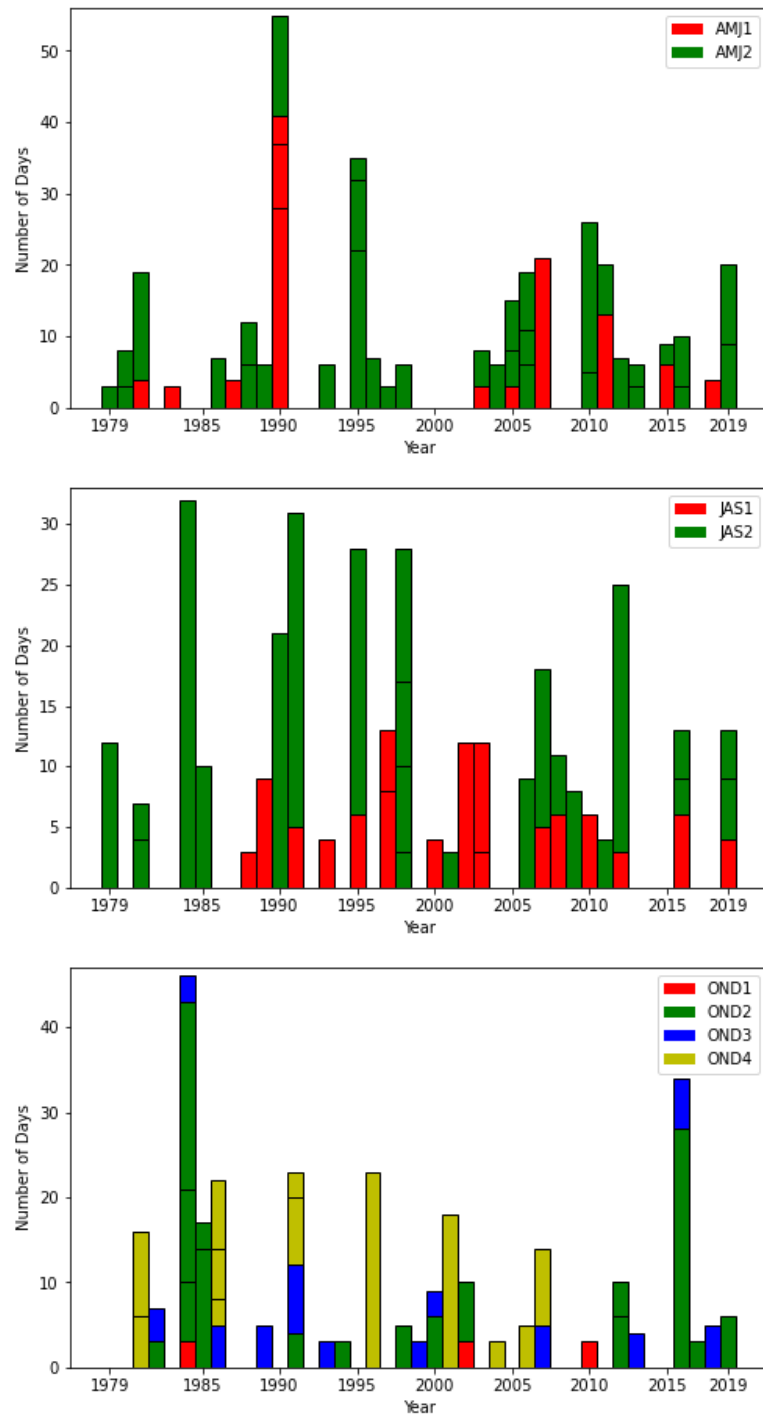


Figure 3.9: Arctic heatwave climatology between 1979 and 2019 for spring (top), summer (medium) and autumn (bottom) clusters. The horizontal black segments separate single events.

3.3 Heatwave intensity and duration

To conclude Chapter 3, this Section examines whether heatwave time lengths and intensities are correlated and how they change across the four seasons and the different clusters.

Figure 3.10 provides an overall view very useful to investigate these themes. The most evident feature is the large difference in intensity between the different seasons. Indeed, the summer mean intensity (1.25 K) is less than 30% of the winter one (4.31 K). Spring and autumn mean values are 2.20 K and 3.53 K , respectively. Seasonal variations of heatwave duration are less marked then end of opposite sign to the intensity ones; seasonal mean time lengths are, in ascending order, 6.3 (JFM), 6.9 (OND), 7.5 (AMJ) and 8.4 (JAS) days. There are only 15 events (about 8.3% of the total) lasting more than 14 days and only one of them occurs in winter.

These results are not particularly surprising given the higher weather variability of autumn and winter with respect to spring and summer.

The heatwave magnitude was defined as the product of intensity and duration in Section 2.1; its seasonal mean values testify the stronger character of winter and autumn events: 28.76 (JFM), 27.10 (OND), 19.17 (AMJ) and 12.27 (JAS) $K \cdot d$.

Typically for each single season clusters with higher duration have also higher intensity (the only exception is OND4, probably due to the fact that its highest warm anomalies are outside the high Arctic and therefore do not influence the intensity calculation [see Section 2.1]). Furthermore, in every cluster of each season intensity and duration result positively correlated ($0.36 \leq r \leq 0.91$). Consequently this is true for every season taken as a whole, for which the four correlation coefficient are all greater than 0.6 (statistically extremely significant).

According to a linear fit the faster growth in intensity increasing duration is observed in winter (0.14 K/d), whereas the lowest one in summer (0.04 K/d).

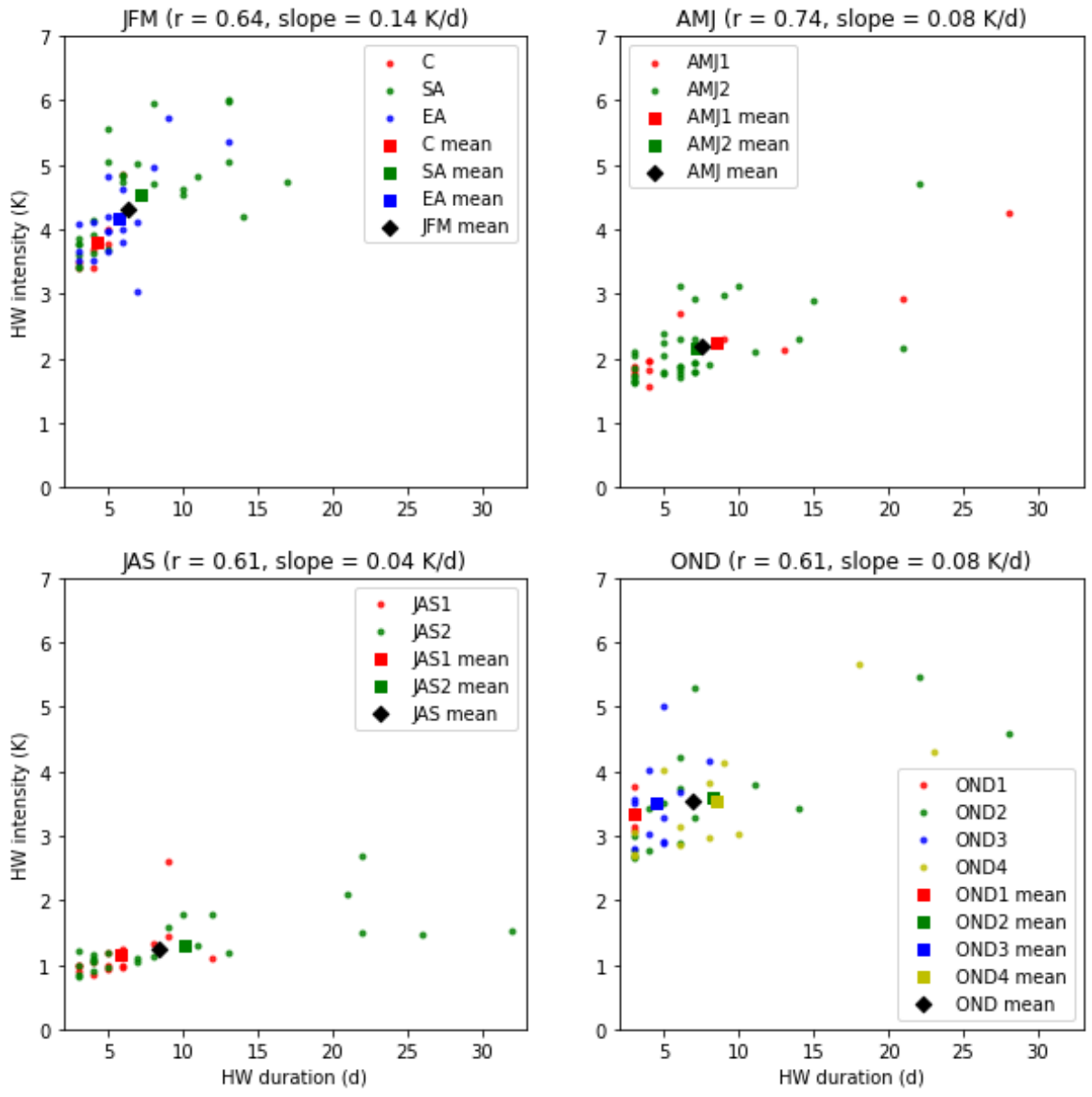


Figure 3.10: Scatterplots of the heatwave events, divided in the four seasons (JFM, AMJ, JAS, OND), with the duration (in days) in abscissa and the intensity (in K) in ordinate. Squares denote clusters' mean values, black rhombuses denote seasonal mean values. On the top of each panel the corresponding seasonal correlation coefficient and slope of the linear fit is reported.

4 | Discussion

In Section 1.3 the principal physical mechanisms that, according to several recent studies, lead to Arctic warm extremes have been reported: moist intrusions, subsiding air masses during blocking events, marine cold air outbreaks and meridional transport. On the basis of them, in this Chapter some interpretations of the clusters' circulation features and temperature patterns illustrated in Chapter 3 are suggested.

Kapsch et al. 2013 [53] showed that in years where the end-of-summer sea-ice extent is well below normal, a significantly enhanced transport of humid air is evident during spring into the region where the ice retreat is encountered. This enhanced transport of moist air leads to an anomalous convergence of humidity, and to an increase of the cloudiness. The increase of the cloudiness and humidity results in an enhancement of the greenhouse effect that plays a significant role in initiating the summer ice melt [53]. AMJ1 seems to be caused by these spring injections since it presents a meridional path, formed by two opposite 500-*hPa* geopotential height anomalies, that is particularly suited for transporting warm humid air from the Atlantic to the high Arctic (Figure 3.6). As a confirmation of this the temperature anomaly peaks over the end of the aforesaid path. Therefore AMJ1 may be the immediate effect of episodes of intense meridional moisture flux, that are very important in triggering ice melting.

Anticipated spring sea ice melting renders more efficient the absorption of enhanced downward shortwave radiation during summer anticyclone events, in which downwelling leads to adiabatic warming and reduced cloudiness. Wernli and Papritz 2018 [135] analysed summer Arctic anticyclones and revealed that sea ice reduction is systematically enhanced during these transient episodes. Moreover, the seasonal reduction of sea ice volume correlates with the area-averaged frequency of summer Arctic anticyclones poleward of 70°N (correlation coefficient of 0.57) [135]. According to Ogi and Wallace 2012 [81] anomalous and sustained low-level winds associated with these anticyclones may also contribute to enhanced export and mechanical break-up of thin ice. Furthermore, Papritz 2019 [86] showed elevated blocking frequency over the high Arctic in correspondence of summer (JJA) warm extremes and demonstrated the dominant role of subsiding air masses in this latter (Figure 1.8). Therefore, JAS2, whose mean duration (10 days) equals that of summer anticyclones identified in Wernli and Papritz 2018 [135], is probably

mainly caused by subsidence during blocking events. Presumably also AMJ2 is due to the same dynamic. Wernli and Papritz 2018 [135] asserted that these anticyclones are formed through injections of air masses with low potential vorticity into the Arctic upper troposphere by lower latitude cyclones and that about half of this transport is associated with intense latent heating in the cyclones' cloud systems (warm conveyor belt).

A prominent role of anticyclonic anomalies in causing Arctic heatwaves is evident also in autumn for clusters OND1 and OND2, and in winter for clusters SA and EA, that together account for 86% of winter events.

Papritz 2019 [86] found that three types of air masses are important in producing winter (DJF) warm extremes north to 80°N (Figure 1.8): subsiding (about 40%), diabatically heated (typically in marine cold air outbreaks; about 40%) and poleward-moving warm (about 20%) air masses. An interesting question is whether each different cluster reflect primarily one of these dynamics or not. Here some considerations in favor of this hypothesis are made, but more specific studies are necessary to draw conclusions in this regard.

Even if warm advection from the Atlantic likely contributes, EA may be mostly due to subsidence during blocking events given that its anticyclonic anomaly is centered over the area with maximum positive anomaly of blocking frequency during winter warm extremes [86]. Moreover, it is precisely in this area that subsiding air masses mainly originates, as shown in Figure 1.9 (e).

Instead, marine cold air outbreaks (MCAOs) could be the major cause of SA through the advection of cold Siberian air, warmed by strong upward sensible heat flux over the Barents Sea (ice-free during all the year), to the North Pole. This path is consistent with the position of the anticyclonic anomaly in SA (Figure 3.2) and with the results of Papritz 2019 [86] shown in Figure 1.9 (d). Although to a lesser extent, another MCAO path that could contribute in determining SA events is the one originating over Canada, heated over the Atlantic and steered to the Arctic by the cyclonic anomaly peaked over the Irminger Sea (Figure 3.2).

This latter North American MCAO path probably plays an important role also in cluster OND3, together with transport of already warm air from southern and western Europe. Indeed, OND3 presents a straight meridional path across the north-eastern Atlantic, formed by the opposition of a cyclonic anomaly over the Irminger Sea and an anticyclonic one over northern Europe, that is particularly suited for intrusions of warm and humid air from lower latitudes (Figure 3.8). Also the warm anomaly position support this thesis. Another cluster for which transport of already warm air masses from lower latitudes seems to play a key role is C (Figure 3.2 and 3.3). In this case the most common mechanism could be the joint action of an anticyclonic anomaly over central-northern Europe with Atlantic and/or polar cyclonic systems. This interplay could be effective in transporting warm moist air from southern North Atlantic and the Mediterranean region toward the Eurasian sector of the Arctic, where the mean temperature anomaly is higher.

Furthermore, Ruggieri et al. [106] showed that blocking over Scandinavia can steer to the

north the Atlantic storm track, strongly enhancing the meridional heat transport across Greenland and Norwegian Seas. This process could be relevant for clusters OND3 and C.

As regards possible significant decadal variability in the occurrence of winter clusters (Figure 3.4), preliminary observations suggest a negative correlation for EA and slight positive correlation for SA with the Arctic Oscillation (AO) to be confirmed by ulterior, more specific analyses. It would be interesting to investigate, on a more extended study period, eventual relations with the Atlantic Multidecadal Oscillation (AMO), that is the principal mode of variability in the Northern Hemisphere and has large influence on many atmospheric phenomena (e.g. Dehai Luo et al. 2017 [66]; Li et al. 2018 [63]; Chen et al. 2020 [17]).

In the present study the succession of the different winter event types (Figure 3.4) becomes more homogeneous in correspondence of the strong Arctic warming trend started approximately in 2005 (Figure 2.1). So, another aspect to explore is whether temperature trends can cause any changes in the frequency of occurrence of the different clusters.

Finally, another possible future work useful for further comprehend Arctic warm extremes could be to consider also heatwaves with a lesser spatial extent than those investigated in this thesis work and to classify the heatwaves on the base of their temperature (instead that geopotential height) pattern anomaly. To do so, a heatwave definition tailored for this purpose should be used. In particular, a modified version of the definition designed by Stefanon et al. [122] (see Section 1.1) could be utilized. In this new definition the grid-point threshold could be the seasonal 95th percentile of the grid-point temperature anomaly, this latter calculated with the same procedure used in the present study (i.e. with a time-varying climatology, see Section 1.2). Moreover the spatial requirement designed by Stefanon et al. [122] (see Section 1.1), based on squares of side $L=3.75^\circ$, should be changed in order to be area-consistent across the Arctic domain.

A classification of this kind could reveal whether events with a lesser spatial extent than those investigated in this thesis work are important or not. Otherwise, it could confirm the results obtained in this study.

Moreover, it could be performed on a broader domain in order to consider also continental Arctic regions.

5 | Conclusions

In the last decades the interest of the scientific community on Arctic warm extremes has been growing due to their multiple (climatic, ecosystemic and socioeconomic) impacts both on local and global scales. So far, these events have been studied mainly individually or through their mean characteristics relative to a single season (mostly winter). The objective of this study was to identify, separately for each of the four seasons, the different large scale circulation drivers and the corresponding features (temperature pattern, intensity, duration) of Arctic warm extremes.

A definition of Arctic heatwave (over the domain poleward to 75°N) was formulated using temperature anomalies obtained from a time-dependent climatology designed by Messori et al. 2018 [73] for identify Arctic warm extremes. A percentile threshold and a minimum duration have been used as amplitude and persistence requirements, respectively, in accordance with the most common structure of heatwave definitions in scientific literature. According to this definition and using 2-*m* temperature data from the last generation reanalysis ERA5 (produced by ECMWF) 180 heatwave events are detected among all seasons in the period 1979-2019.

Then these events have been classified, for each single season, on the base of their 500-*hPa* geopotential height anomaly patterns from 30°N to 90°N with a hierarchical clustering algorithm in order to identify the different large scale circulation regimes typical of Arctic heatwaves.

The principal findings are set out below.

From the winter (JFM) classification three different clusters emerge. Two of them account for the vast majority of the events (44/51) and presents a 500-*hPa* geopotential height anomaly dipole structure over the Arctic, formed by a pronounced high latitude anticyclonic anomaly in the Eurasian sector and a cyclonic less marked one in the North American sector. These two principal patterns differ essentially for a partial rotation ($\sim 70^\circ$) of the abovementioned geopotential dipole and are named on the base of the anticyclonic pole's position: in SA (Siberian anticyclonic) the positive geopotential anomaly peaks over Severnaya Zemlya, favouring advection from Siberia, whereas in EA (Eurasian anticyclonic) peaks over the Barents and Kara Seas and stretches toward the Norwegian Sea, favouring advection from the Atlantic.

Both configurations show a strong warm anomaly peaked in the region between Svalbard,

Franz Joseph Land and the North Pole, and an extensive smoother cold anomaly over central and western Siberia. This temperature configuration resembles the well known WACE (warm Arctic-cold Eurasia) pattern that characterized the winter seasons of the last two decades and attracted considerable attention in the climate research community because unexpected cold winters in Eurasia have caused severe damage to livelihoods and socio-ecological systems (Nandintsetseg et al. 2018 [79]). The main temperature differences are that in EA also European Russia experience a significant cooling and that North America presents opposite (but not pronounced) temperature anomalies in the two cases (positive in EA, negative in SA).

The third winter cluster is composed by 7 short-lived, less intense heatwaves and is countersigned by the prevalent presence of cyclonic anomalies in the Arctic. Atlantic and polar cyclonic activity may play a crucial role in causing its warm anomaly, located in the Eurasian sector too.

The observation of the three winter patterns together with the results obtained by Papritz 2019 [86] suggests that different clusters may correspond to different thermodynamic evolution of the air masses that cause the temperature extreme, but further studies are needed to verify this hypothesis.

As regards the other seasons, in all of them the cluster composed by the highest number of heatwaves is characterized by an anticyclonic monopole over the high Arctic. Therefore high latitude anticyclones result to be the main driver of Arctic heatwaves (typically of above average duration) in all the four seasons.

Furthermore, both in spring (AMJ) and autumn (OND) another circulation regime results important. This latter is dominated by a geopotential dipole structure over northern Atlantic that determines a strong advection from the Atlantic to the high Arctic, in which the warm anomaly reaches its maximum.

Heatwave duration and intensity result positively correlated ($r > 0.6$) in every single season and the greater increment in intensity increasing duration is observed in winter. There is a considerable difference in the intensities between the different seasons, with winter (JFM) ones averagely more than three times greater than summer (JAS) ones. Heatwaves with high magnitude, defined as the product of intensity and duration, occur mainly in winter and autumn.

The temporal series of the different types of heatwave do not point out evident periodicities or variations in the their frequency of occurrence during the study period for spring, summer and autumn.

This cannot be said for winter: the first decade of the study period was dominated by EA events, whereas the subsequent 10-15 years were characterize by SA heatwaves. Otherwise the final part of the time series shows a more balanced succession of the three heatwaves types. Further study are necessary to comprehend whether this decadal variations are linked with any important climatic mode of variability (such as the Arctic Oscillation, as a preliminary inspection suggests, or the Atlantic Multidecadal Oscillation) and whether the temperature trend plays a relevant role.

In order to answer these latter questions and to verify whether the different circulation regimes identified here are stable on a longer temporal extent, it would be important to repeat the analysis extending the study period further back in time. Finally, another interesting work could be to see whether with preindustrial control (PIC) simulations essentially the same classification is obtained, in order to understand whether the heatwave circulation regimes are sensible to variations in the climate forcings or not.

Acknowledgements

First I would like to thank my thesis supervisor Prof. Paolo Ruggieri for its precious and precise support and for its careful guide despite the difficult pandemic period. Then I would like to thank Prof. Silvana Di Sabatino for orientating me in the final part of my university career.

Furthermore, I thank all my fantastic university mates that rendered the journey gentle, stimulating and enjoyable. A big thank goes also to my friends from Romagna and to my theater fellows, that were both fundamental for my personal growth and well-being.

Moreover, I thank my girlfriend Giulia for filling my life and for sharing with me both beautiful and bad moments.

Finally, I especially thank my family for having always supported me, for being a stable point of reference and for having always helped me during difficulties.

References

- [1] Y. Aksenov, E. E. Popova, A. Yool, A. J. G. Nurser, T. D. Williams, L. Bertino, and J. Bergh. On the future navigability of Arctic sea routes: High-resolution projections of the Arctic Ocean and sea ice. *Marine Policy*, 75:300–317, 2017. ISSN 0308-597X. doi:<https://doi.org/10.1016/j.marpol.2015.12.027>.
- [2] B. G. Anderson and M. L. Bell. Weather-related mortality: how heat, cold, and heat waves affect mortality in the United States. *Epidemiology (Cambridge, Mass.)*, 20(2):205–213, mar 2009. ISSN 1531-5487. doi:10.1097/EDE.0b013e318190ee08.
- [3] T. W. K. Armitage, G. E. Manucharyan, A. A. Petty, R. Kwok, and A. F. Thompson. Enhanced eddy activity in the Beaufort Gyre in response to sea ice loss. *Nature Communications*, 11(1):761, 2020. ISSN 2041-1723. doi:10.1038/s41467-020-14449-z.
- [4] S. Arrhenius. XXXI. On the influence of carbonic acid in the air upon the temperature of the ground. *The London, Edinburgh, and Dublin Philosophical Magazine and Journal of Science*, 41(251):237–276, apr 1896. ISSN 1941-5982. doi:10.1080/14786449608620846.
- [5] C. Baggett and S. Lee. Arctic Warming Induced by Tropically Forced Tapping of Available Potential Energy and the Role of the Planetary-Scale Waves. *Journal of the Atmospheric Sciences*, 72(4):1562–1568, 2015. doi:10.1175/JAS-D-14-0334.1.
- [6] C. Baggett, S. Lee, and S. Feldstein. An Investigation of the Presence of Atmospheric Rivers over the North Pacific during Planetary-Scale Wave Life Cycles and Their Role in Arctic Warming. *Journal of the Atmospheric Sciences*, 73(11):4329–4347, 2016. doi:10.1175/JAS-D-16-0033.1.
- [7] E. Barcena-Martin, J. Molina, and J. D. Ruiz-Sinoga. Issues and challenges in defining a heat wave: A Mediterranean case study. *International Journal of Climatology*, 39(2):331–342, jan 2019. ISSN 0899-8418. doi:<https://doi.org/10.1002/joc.5809>.
- [8] K. M. Barlow, B. P. Christy, G. J. O’Leary, P. A. Riffkin, and J. G. Nuttall. Simulating the impact of extreme heat and frost events on wheat crop produc-

- tion: A review. *Field Crops Research*, 171:109–119, 2015. ISSN 0378-4290. doi:<https://doi.org/10.1016/j.fcr.2014.11.010>.
- [9] E. A. Barnes, E. Dunn-Sigouin, G. Masato, and T. Woollings. Exploring recent trends in Northern Hemisphere blocking. *Geophysical Research Letters*, 41(2): 638–644, jan 2014. ISSN 0094-8276. doi:<https://doi.org/10.1002/2013GL058745>.
- [10] D. Barriopedro, E. M. Fischer, J. Luterbacher, R. M. Trigo, and R. García-Herrera. The Hot Summer of 2010: Redrawing the Temperature Record Map of Europe. *Science*, 332(6026):220, apr 2011. doi:10.1126/science.1201224.
- [11] M. Beniston. Warm winter spells in the Swiss Alps: Strong heat waves in a cold season? A study focusing on climate observations at the Saentis high mountain site. *Geophysical Research Letters*, 32(1), jan 2005. ISSN 0094-8276. doi:<https://doi.org/10.1029/2004GL021478>.
- [12] M. Beniston, D. B. Stephenson, O. B. Christensen, C. A. T. Ferro, C. Frei, S. Goyette, K. Halsnaes, T. Holt, K. Jylhä, B. Koffi, J. Palutikof, R. Schöll, T. Semmler, and K. Woth. Future extreme events in European climate: an exploration of regional climate model projections. *Climatic Change*, 81(1):71–95, 2007. ISSN 1573-1480. doi:10.1007/s10584-006-9226-z.
- [13] R. Bintanja, R. G. Graversen, and W. Hazeleger. Arctic winter warming amplified by the thermal inversion and consequent low infrared cooling to space. *Nature Geoscience*, 4(11):758–761, 2011. ISSN 1752-0908. doi:10.1038/ngeo1285.
- [14] G. J. Boer and S. J. Lambert. Second-order space-time climate difference statistics. *Climate Dynamics*, 17(2):213–218, 2001. ISSN 1432-0894. doi:10.1007/PL00013735.
- [15] E. C. Carmack and H. Melling. Warmth from the deep. *Nat. Geosci.*, 4:7–8, 2011.
- [16] J. Cattiaux, R. Vautard, C. Cassou, P. Yiou, V. Masson-Delmotte, and F. Codron. Winter 2010 in Europe: A cold extreme in a warming climate. *Geophysical Research Letters*, 37(20), oct 2010. ISSN 0094-8276. doi:<https://doi.org/10.1029/2010GL044613>.
- [17] S. Chen, W. Chen, R. Wu, and L. Song. Impacts of the Atlantic Multidecadal Oscillation on the Relationship of the Spring Arctic Oscillation and the Following East Asian Summer Monsoon. *Journal of Climate*, 33(15):6651–6672, 2020. doi:10.1175/JCLI-D-19-0978.1.
- [18] X. Cheng and J. M. Wallace. Cluster Analysis of the Northern Hemisphere Wintertime 500-hPa Height Field: Spatial Patterns. *Journal of Atmospheric Sciences*, 50(16):2674–2696, 1993. doi:10.1175/1520-0469(1993)050<2674:CAOTNH>2.0.CO;2.

- [19] H. N. Cheung, W. Zhou, Y. Shao, W. Chen, H. Y. Mok, and M. C. Wu. Observational climatology and characteristics of wintertime atmospheric blocking over Ural–Siberia. *Climate Dynamics*, 41(1):63–79, 2013. ISSN 1432-0894. doi:10.1007/s00382-012-1587-6.
- [20] D.-J. Cho and K.-Y. Kim. Role of Ural blocking in Arctic sea ice loss and its connection with Arctic warming in winter. *Climate Dynamics*, 2020. ISSN 1432-0894. doi:10.1007/s00382-020-05545-3.
- [21] P. Ciais, M. Reichstein, N. Viovy, A. Granier, J. Ogee, V. Allard, M. Aubinet, N. Buchmann, C. Bernhofer, A. Carrara, F. Chevallier, N. De Noblet, A. D. Friend, P. Friedlingstein, T. Grünwald, B. Heinesch, P. Keronen, A. Knohl, G. Krinner, D. Loustau, G. Manca, G. Matteucci, F. Miglietta, J. M. Ourcival, D. Papale, K. Pilegaard, S. Rambal, G. Seufert, J. F. Soussana, M. J. Sanz, E. D. Schulze, T. Vesala, and R. Valentini. Europe-wide reduction in primary productivity caused by the heat and drought in 2003. *Nature*, 437(7058):529–533, 2005. ISSN 1476-4687. doi:10.1038/nature03972.
- [22] J. Cohen, J. A. Screen, J. C. Furtado, M. Barlow, D. Whittleston, D. Coumou, J. Francis, K. Dethloff, D. Entekhabi, J. Overland, and J. Jones. Recent Arctic amplification and extreme mid-latitude weather. *Nature Geoscience*, 7(9):627–637, 2014. ISSN 1752-0908. doi:10.1038/ngeo2234.
- [23] A. F. Colombo, D. Etkin, and B. W. Karney. Climate Variability and the Frequency of Extreme Temperature Events for Nine Sites across Canada: Implications for Power Usage. *Journal of Climate*, 12(8):2490–2502, 1999. doi:10.1175/1520-0442(1999)012<2490:CVATFO>2.0.CO;2.
- [24] D. Coumou and S. Rahmstorf. A decade of weather extremes. *Nature Climate Change*, 2(7):491–496, 2012. ISSN 1758-6798. doi:10.1038/nclimate1452.
- [25] M. Croci-Maspoli and H. C. Davies. Key Dynamical Features of the 2005/06 European Winter. *Monthly Weather Review*, 137(2):664–678, 2009. doi:10.1175/2008MWR2533.1.
- [26] R. E. Davis, G. R. McGregor, and K. B. Enfield. Humidity: A review and primer on atmospheric moisture and human health. *Environmental Research*, 144:106–116, 2016. ISSN 0013-9351. doi:https://doi.org/10.1016/j.envres.2015.10.014.
- [27] Y. Depietri, F. G. Renaud, and G. Kallis. Heat waves and floods in urban areas: a policy-oriented review of ecosystem services. *Sustainability science*, 7(1):95–107, 2012. ISSN 1862-4065.

- [28] Q. Ding, A. Schweiger, M. L’Heureux, D. S. Battisti, S. Po-Chedley, N. C. Johnson, E. Blanchard-Wrigglesworth, K. Harnos, Q. Zhang, R. Eastman, and E. J. Steig. Influence of high-latitude atmospheric circulation changes on summertime Arctic sea ice. *Nature Climate Change*, 7(4):289–295, 2017. ISSN 1758-6798. doi:10.1038/nclimate3241.
- [29] A. Dufour, O. Zolina, and S. K. Gulev. Atmospheric Moisture Transport to the Arctic: Assessment of Reanalyses and Analysis of Transport Components. *Journal of Climate*, 29(14):5061–5081, 2016. doi:10.1175/JCLI-D-15-0559.1.
- [30] R. J. H. Dunn, N. E. Mead, K. M. Willett, and D. E. Parker. Analysis of heat stress in UK dairy cattle and impact on milk yields. *Environmental Research Letters*, 9(6):064006, 2014. ISSN 1748-9326. doi:10.1088/1748-9326/9/6/064006.
- [31] E. Durbin, R. G. Campbell, M. C. Casas, B. Niehoff, J. Runge, and M. Wagner. Interannual variation in phytoplankton blooms and zooplankton productivity and abundance in the Gulf of Maine during winter. *Marine Ecology-progress Series - MAR ECOL-PROGR SER*, 254:81–100, jun 2003. doi:10.3354/meps254081.
- [32] V. M. Eguíluz, J. Fernández-Gracia, X. Irigoien, and C. M. Duarte. A quantitative assessment of Arctic shipping in 2010–2014. *Scientific Reports*, 6(1):30682, 2016. ISSN 2045-2322. doi:10.1038/srep30682.
- [33] A. H. Fink, T. Brücher, A. Krüger, G. C. Leckebusch, J. G. Pinto, and U. Ulbrich. The 2003 European summer heatwaves and drought –synoptic diagnosis and impacts. *Weather*, 59(8):209–216, aug 2004. ISSN 0043-1656. doi:https://doi.org/10.1256/wea.73.04.
- [34] E. M. Fischer and C. Schär. Consistent geographical patterns of changes in high-impact European heatwaves. *Nature Geoscience*, 3(6):398–403, 2010. ISSN 1752-0908. doi:10.1038/ngeo866.
- [35] M. D. Flournoy, S. B. Feldstein, S. Lee, and E. E. Clothiaux. Exploring the Tropically Excited Arctic Warming Mechanism with Station Data: Links between Tropical Convection and Arctic Downward Infrared Radiation. *Journal of the Atmospheric Sciences*, 73(3):1143–1158, 2016. doi:10.1175/JAS-D-14-0271.1.
- [36] J. A. Francis and E. Hunter. Changes in the fabric of the Arctic’s greenhouse blanket. *Environmental Research Letters*, 2(4):045011, 2007. ISSN 1748-9326. doi:10.1088/1748-9326/2/4/045011.
- [37] J. A. Francis and S. J. Vavrus. Evidence for a wavier jet stream in response to rapid Arctic warming. *Environmental Research Letters*, 10(1):014005, 2015. ISSN 1748-9326. doi:10.1088/1748-9326/10/1/014005.

- [38] A. Gershunov, D. R. Cayan, and S. F. Iacobellis. The Great 2006 Heat Wave over California and Nevada: Signal of an Increasing Trend. *Journal of Climate*, 22(23): 6181–6203, 2009. doi:10.1175/2009JCLI2465.1.
- [39] M. Goss, S. B. Feldstein, and S. Lee. Stationary Wave Interference and Its Relation to Tropical Convection and Arctic Warming. *Journal of Climate*, 29(4):1369–1389, 2016. doi:10.1175/JCLI-D-15-0267.1.
- [40] R. M. Graham, S. R. Hudson, and M. Maturilli. Improved Performance of ERA5 in Arctic Gateway Relative to Four Global Atmospheric Reanalyses. *Geophysical Research Letters*, 46(11):6138–6147, jun 2019. ISSN 0094-8276. doi:https://doi.org/10.1029/2019GL082781.
- [41] R. G. Graversen and M. Burtu. Arctic amplification enhanced by latent energy transport of atmospheric planetary waves. *Quarterly Journal of the Royal Meteorological Society*, 142(698):2046–2054, jul 2016. ISSN 0035-9009. doi:https://doi.org/10.1002/qj.2802.
- [42] R. G. Graversen, P. L. Langen, and T. Mauritsen. Polar Amplification in CCSM4: Contributions from the Lapse Rate and Surface Albedo Feedbacks. *Journal of Climate*, 27(12):4433–4450, 2014. doi:10.1175/JCLI-D-13-00551.1.
- [43] C. H. Greene and A. J. Pershing. Climate Drives Sea Change. *Science*, 315(5815): 1084, feb 2007. doi:10.1126/science.1136495. URL <http://science.sciencemag.org/content/315/5815/1084.abstract>.
- [44] C. H. Greene, A. J. Pershing, T. M. Cronin, and N. Ceci. ARCTIC CLIMATE CHANGE AND ITS IMPACTS ON THE ECOLOGY OF THE NORTH ATLANTIC. *Ecology*, 89(sp11):S24–S38, nov 2008. ISSN 0012-9658. doi:https://doi.org/10.1890/07-0550.1.
- [45] H. Hersbach, B. Bell, P. Berrisford, G. Biavati, A. Horányi, J. Muñoz Sabater, J. Nicolas, C. Peubey, R. Radu, I. Rozum, D. Schepers, A. Simmons, C. Soci, D. Dee, and J.-N. Thépaut. ERA5 hourly data on pressure levels from 1979 to present. *Copernicus Climate Change Service (C3S) Climate Data Store (CDS)*, 2018. doi:https://doi.org/10.24381/cds.bd0915c6.
- [46] H. Hersbach, B. Bell, P. Berrisford, G. Biavati, A. Horányi, J. Muñoz Sabater, J. Nicolas, C. Peubey, R. Radu, I. Rozum, D. Schepers, A. Simmons, C. Soci, D. Dee, and J.-N. Thépaut. ERA5 hourly data on single levels from 1979 to present. *Copernicus Climate Change Service (C3S) Climate Data Store (CDS)*, 2018. doi:https://doi.org/10.24381/cds.adbb2d47.

- [47] H. Hersbach, B. Bell, P. Berrisford, S. Hirahara, A. Horányi, J. Muñoz-Sabater, J. Nicolas, C. Peubey, R. Radu, D. Schepers, A. Simmons, C. Soci, S. Abdalla, X. Abellan, G. Balsamo, P. Bechtold, G. Biavati, J. Bidlot, M. Bonavita, G. De Chiara, P. Dahlgren, D. Dee, M. Diamantakis, R. Dragani, J. Flemming, R. Forbes, M. Fuentes, A. Geer, L. Haimberger, S. Healy, R. J. Hogan, E. Hólm, M. Janisková, S. Keeley, P. Laloyaux, P. Lopez, C. Lupu, G. Radnoti, P. de Rosnay, I. Rozum, F. Vamborg, S. Villaume, and J.-N. Thépaut. The ERA5 global reanalysis. *Quarterly Journal of the Royal Meteorological Society*, 146(730):1999–2049, jul 2020. ISSN 0035-9009. doi:<https://doi.org/10.1002/qj.3803>.
- [48] M. Honda, J. Inoue, and S. Yamane. Influence of low Arctic sea-ice minima on anomalously cold Eurasian winters. *Geophysical Research Letters*, 36(8), apr 2009. ISSN 0094-8276. doi:<https://doi.org/10.1029/2008GL037079>.
- [49] S. Hopsch, J. Cohen, and K. Dethloff. Analysis of a link between fall Arctic sea ice concentration and atmospheric patterns in the following winter. *Tellus A: Dynamic Meteorology and Oceanography*, 64(1):18624, dec 2012. ISSN null. doi:10.3402/tellusa.v64i0.18624.
- [50] R. M. Horton, J. S. Mankin, C. Lesk, E. Coffel, and C. Raymond. A Review of Recent Advances in Research on Extreme Heat Events. *Current Climate Change Reports*, 2(4):242–259, 2016. ISSN 2198-6061. doi:10.1007/s40641-016-0042-x.
- [51] J. Inoue, M. E. Hori, and K. Takaya. The Role of Barents Sea Ice in the Wintertime Cyclone Track and Emergence of a Warm-Arctic Cold-Siberian Anomaly. *Journal of Climate*, 25(7):2561–2568, 2012. doi:10.1175/JCLI-D-11-00449.1.
- [52] D. Johns, M. Edwards, and S. Batten. Arctic boreal plankton species in the Northwest Atlantic. *Canadian Journal of Fisheries and Aquatic Sciences*, 58: 2121–2124, nov 2001. doi:10.1139/cjfas-58-11-2121.
- [53] M.-L. Kapsch, R. G. Graversen, and M. Tjernström. Springtime atmospheric energy transport and the control of Arctic summer sea-ice extent. *Nature Climate Change*, 3(8):744–748, 2013. ISSN 1758-6798. doi:10.1038/nclimate1884.
- [54] R. W. Katz and B. G. Brown. Extreme events in a changing climate: Variability is more important than averages. *Climatic Change*, 21(3):289–302, 1992. ISSN 1573-1480. doi:10.1007/BF00139728.
- [55] B.-M. Kim, J.-Y. Hong, S.-Y. Jun, X. Zhang, H. Kwon, S.-J. Kim, J.-H. Kim, S.-W. Kim, and H.-K. Kim. Major cause of unprecedented Arctic warming in January 2016: Critical role of an Atlantic windstorm. *Scientific Reports*, 7(1):40051, 2017. ISSN 2045-2322. doi:10.1038/srep40051.

- [56] E. M. Knudsen, Y. J. Orsolini, T. Furevik, and K. I. Hodges. Observed anomalous atmospheric patterns in summers of unusual Arctic sea ice melt. *Journal of Geophysical Research: Atmospheres*, 120(7):2595–2611, apr 2015. ISSN 2169-897X. doi:<https://doi.org/10.1002/2014JD022608>.
- [57] H. Koch and S. Vögele. Dynamic modelling of water demand, water availability and adaptation strategies for power plants to global change. *Ecological Economics*, 68(7):2031–2039, 2009. ISSN 0921-8009. doi:<https://doi.org/10.1016/j.ecolecon.2009.02.015>.
- [58] C. Koppe, R. Sari Kovats, B. Menne, G. Jendritzky, W. H. O. R. O. for Europe, L. S. o. H. Medicine, Tropical, E. European Commission. Energy, S. Development, and D. Wetterdienst. Heat-waves : risks and responses / by Christina Koppe ... [et al.], 2004. URL <https://apps.who.int/iris/handle/10665/107552>.
- [59] J.-S. Kug, J.-H. Jeong, Y.-S. Jang, B.-M. Kim, C. K. Folland, S.-K. Min, and S.-W. Son. Two distinct influences of Arctic warming on cold winters over North America and East Asia. *Nature Geoscience*, 8(10):759–762, 2015. ISSN 1752-0908. doi:10.1038/ngeo2517.
- [60] S. B. Lanning, T. J. Siebenmorgen, P. A. Counce, A. A. Ambardekar, and A. Mauroumoustakos. Extreme nighttime air temperatures in 2010 impact rice chalkiness and milling quality. *Field Crops Research*, 124(1):132–136, 2011. ISSN 0378-4290. doi:<https://doi.org/10.1016/j.fcr.2011.06.012>.
- [61] S. Lee. Testing of the Tropically Excited Arctic Warming Mechanism (TEAM) with Traditional El Niño and La Niña. *Journal of Climate*, 25(12):4015–4022, 2012. doi:10.1175/JCLI-D-12-00055.1.
- [62] S. Lee, T. Gong, N. Johnson, S. B. Feldstein, and D. Pollard. On the Possible Link between Tropical Convection and the Northern Hemisphere Arctic Surface Air Temperature Change between 1958 and 2001. *Journal of Climate*, 24(16):4350–4367, 2011. doi:10.1175/2011JCLI4003.1.
- [63] F. Li, Y. J. Orsolini, H. Wang, Y. Gao, and S. He. Atlantic Multidecadal Oscillation Modulates the Impacts of Arctic Sea Ice Decline. *Geophysical Research Letters*, 45(5):2497–2506, mar 2018. ISSN 0094-8276. doi:<https://doi.org/10.1002/2017GL076210>.
- [64] C. Liu and E. A. Barnes. Extreme moisture transport into the Arctic linked to Rossby wave breaking. *Journal of Geophysical Research: Atmospheres*, 120(9):3774–3788, may 2015. ISSN 2169-897X. doi:<https://doi.org/10.1002/2014JD022796>.

- [65] B. Luo, D. Luo, L. Wu, L. Zhong, and I. Simmonds. Atmospheric circulation patterns which promote winter Arctic sea ice decline. *Environmental Research Letters*, 12(5):054017, 2017. ISSN 1748-9326. doi:10.1088/1748-9326/aa69d0.
- [66] D. Luo, Y. Chen, A. Dai, M. Mu, R. Zhang, and S. Ian. Winter Eurasian cooling linked with the Atlantic Multidecadal Oscillation. *Environmental Research Letters*, 12(12):125002, 2017. ISSN 1748-9326. doi:10.1088/1748-9326/aa8de8.
- [67] J. Luterbacher, D. Dietrich, E. Xoplaki, M. Grosjean, and H. Wanner. European Seasonal and Annual Temperature Variability, Trends, and Extremes Since 1500. *Science*, 303(5663):1499, mar 2004. doi:10.1126/science.1093877.
- [68] H. Matthes, A. Rinke, and K. Dethloff. Recent changes in Arctic temperature extremes: warm and cold spells during winter and summer. *Environmental Research Letters*, 10(11):114020, 2015. ISSN 1748-9326. doi:10.1088/1748-9326/10/11/114020.
- [69] A. Matzarakis and P. T. Nastos. Human-biometeorological assessment of heat waves in Athens. *Theoretical and applied climatology*, 105(1-2):99–106, 2011. ISSN 0177-798X.
- [70] D. McEvoy, I. Ahmed, and J. Mullett. The impact of the 2009 heat wave on Melbourne’s critical infrastructure. *Local Environment*, 17(8):783–796, sep 2012. ISSN 1354-9839. doi:10.1080/13549839.2012.678320.
- [71] A. J. McMichael and E. Lindgren. Climate change: Present and future risks to health, and necessary responses. *Journal of internal medicine*, 270:401–413, jun 2011. doi:10.1111/j.1365-2796.2011.02415.x.
- [72] L. O. Mearns, R. W. Katz, and S. H. Schneider. Extreme High-Temperature Events: Changes in their Probabilities with Changes in Mean Temperature. *Journal of Climate and Applied Meteorology*, 23(12):1601–1613, 1984. ISSN 07333021, 21635366. URL <http://www.jstor.org/stable/26181141>.
- [73] G. Messori, C. Woods, and R. Caballero. On the Drivers of Wintertime Temperature Extremes in the High Arctic. *Journal of Climate*, 31(4):1597–1618, 2018. doi:10.1175/JCLI-D-17-0386.1.
- [74] S. Miller, R. Muir-Wood, and A. Boissonnade. An exploration of trends in normalized weather-related catastrophe losses. In H. F. Diaz and R. J. Murnane, editors, *Climate Extremes and Society*, pages 225–247. Cambridge University Press, Cambridge, 2008. ISBN 9780521870283. doi:DOI: 10.1017/CBO9780511535840.015.
- [75] K. E. Mills, A. J. Pershing, C. J. Brown, Y. Chen, F.-S. Chiang, D. S. Holland, S. Lehuta, J. A. Nye, J. C. Sun, A. C. Thomas, and R. A. Wahle. Fisheries

- management in a changing climate: Lessons from the 2012 ocean heat wave in the Northwest Atlantic. *Oceanography*, 26(2), 2013. doi:10.5670/oceanog.2013.27.
- [76] G. W. K. Moore. The December 2015 North Pole Warming Event and the Increasing Occurrence of Such Events. *Scientific Reports*, 6(1):39084, 2016. ISSN 2045-2322. doi:10.1038/srep39084.
- [77] M. Mori, M. Watanabe, H. Shiogama, J. Inoue, and M. Kimoto. Robust Arctic sea-ice influence on the frequent Eurasian cold winters in past decades. *Nature Geoscience*, 7(12):869–873, 2014. ISSN 1752-0908. doi:10.1038/ngeo2277.
- [78] T. Naakka, T. Nygård, T. Vihma, J. Sedlar, and R. Graversen. Atmospheric moisture transport between mid-latitudes and the Arctic: Regional, seasonal and vertical distributions. *International Journal of Climatology*, 39(6):2862–2879, may 2019. ISSN 0899-8418. doi:https://doi.org/10.1002/joc.5988.
- [79] B. Nandintsetseg, M. Shinoda, C. Du, and E. Munkhjargal. Cold-season disasters on the Eurasian steppes: Climate-driven or man-made. *Scientific Reports*, 8(1):14769, 2018. ISSN 2045-2322. doi:10.1038/s41598-018-33046-1.
- [80] N. Nicholls, B. Lavery, C. Frederiksen, W. Drosowsky, and S. Torok. Recent apparent changes in relationships between the El Niño-Southern Oscillation and Australian rainfall and temperature. *Geophysical Research Letters*, 23(23):3357–3360, nov 1996. ISSN 0094-8276. doi:https://doi.org/10.1029/96GL03166.
- [81] M. Ogi and J. M. Wallace. The role of summer surface wind anomalies in the summer Arctic sea ice extent in 2010 and 2011. *Geophysical Research Letters*, 39(9), may 2012. ISSN 0094-8276. doi:https://doi.org/10.1029/2012GL051330.
- [82] D. Olefeldt, S. Goswami, G. Grosse, D. Hayes, G. Hugelius, P. Kuhry, A. D. McGuire, V. E. Romanovsky, A. B. K. Sannel, E. A. G. Schuur, and M. R. Turetsky. Circumpolar distribution and carbon storage of thermokarst landscapes. *Nature Communications*, 7(1):13043, 2016. ISSN 2041-1723. doi:10.1038/ncomms13043.
- [83] W. H. Organization. Wildfires and heat-wave in the Russian Federation-Public health advice. *WHO, Copenhagen*, 2010.
- [84] S. Outten and I. Esau. A link between Arctic sea ice and recent cooling trends over Eurasia. *Climatic Change*, 110:1069–1075, feb 2012. doi:10.1007/s10584-011-0334-z.
- [85] J. E. Overland, K. R. Wood, and M. Wang. Warm Arctic - cold continents: climate impacts of the newly open Arctic Sea. *Polar Research*, dec 2011. doi:10.3402/polar.v30i0.15787.

- [86] L. Papritz. Arctic Lower-Tropospheric Warm and Cold Extremes: Horizontal and Vertical Transport, Diabatic Processes, and Linkage to Synoptic Circulation Features. *Journal of Climate*, 33(3):993–1016, 2019. doi:10.1175/JCLI-D-19-0638.1.
- [87] D.-S. R. Park, S. Lee, and S. B. Feldstein. Attribution of the Recent Winter Sea Ice Decline over the Atlantic Sector of the Arctic Ocean. *Journal of Climate*, 28(10):4027–4033, 2015. doi:10.1175/JCLI-D-15-0042.1.
- [88] H.-S. Park, S. Lee, S.-W. Son, S. B. Feldstein, and Y. Kosaka. The Impact of Poleward Moisture and Sensible Heat Flux on Arctic Winter Sea Ice Variability. *Journal of Climate*, 28(13):5030–5040, 2015. doi:10.1175/JCLI-D-15-0074.1.
- [89] T.-W. Park, C.-H. Ho, and S. Yang. Relationship between the Arctic Oscillation and Cold Surges over East Asia. *Journal of Climate*, 24(1):68–83, 2011. doi:10.1175/2010JCLI3529.1.
- [90] T. J. Parker, G. J. Berry, and M. J. Reeder. The influence of tropical cyclones on heat waves in Southeastern Australia. *Geophysical Research Letters*, 40(23):6264–6270, dec 2013. ISSN 0094-8276. doi:https://doi.org/10.1002/2013GL058257.
- [91] T. Pearce and B. Smit. 4.23 - Vulnerability and Adaptation to Climate Change in the Canadian Arctic. In R. A. Pielke, editor, *Climate Vulnerability*, pages 293–303. Academic Press, Oxford, 2013. ISBN 978-0-12-384704-1. doi:https://doi.org/10.1016/B978-0-12-384703-4.00439-1.
- [92] S. E. Perkins. A review on the scientific understanding of heat-waves—Their measurement, driving mechanisms, and changes at the global scale. *Atmospheric Research*, 164-165:242–267, 2015. ISSN 0169-8095. doi:https://doi.org/10.1016/j.atmosres.2015.05.014.
- [93] S. E. Perkins and L. V. Alexander. On the Measurement of Heat Waves. *Journal of Climate*, 26(13):4500–4517, 2012. doi:10.1175/JCLI-D-12-00383.1.
- [94] S. E. Perkins-Kirkpatrick and S. C. Lewis. Increasing trends in regional heatwaves. *Nature Communications*, 11(1):3357, 2020. ISSN 2041-1723. doi:10.1038/s41467-020-16970-7.
- [95] A. Pershing, C. Greene, J. Jossi, L. O’Brien, J. Brodziak, and B. Bailey. Inter-decadal variability in the Gulf of Maine zooplankton community with potential impacts on fish recruitment. *ICES Journal of Marine Science*, 62:511–523, oct 2005. doi:10.1016/j.icesjms.2005.04.025.
- [96] V. Petoukhov and V. A. Semenov. A link between reduced Barents-Kara sea ice and cold winter extremes over northern continents. *Journal of*

- Geophysical Research: Atmospheres*, 115(D21), nov 2010. ISSN 0148-0227. doi:<https://doi.org/10.1029/2009JD013568>.
- [97] S. Pfahl and H. Wernli. Quantifying the relevance of atmospheric blocking for co-located temperature extremes in the Northern Hemisphere on (sub-)daily time scales. *Geophysical Research Letters*, 39(12), jun 2012. ISSN 0094-8276. doi:<https://doi.org/10.1029/2012GL052261>.
- [98] C. Photiadou, M. Tye, D. Keellings, and C. Dewes. Modeling European hot spells using extreme value analysis. *Climate Research*, 58, sep 2013. doi:10.3354/cr01191.
- [99] F. Pithan and T. Mauritsen. Arctic amplification dominated by temperature feedbacks in contemporary climate models. *Nature Geoscience*, 7(3):181–184, mar 2014. doi:10.1038/ngeo2071.
- [100] E. Post, U. S. Bhatt, C. M. Bitz, J. F. Brodie, T. L. Fulton, M. Hebblewhite, J. Kerby, S. J. Kutz, I. Stirling, and D. A. Walker. Ecological Consequences of Sea-Ice Decline. *Science*, 341(6145):519–524, 2013. ISSN 0036-8075. doi:10.1126/science.1235225.
- [101] J. F. Quinting and M. J. Reeder. Southeastern Australian Heat Waves from a Trajectory Viewpoint. *Monthly Weather Review*, 145(10):4109–4125, 2017. doi:10.1175/MWR-D-17-0165.1.
- [102] P. Reid and G. Beaugrand. Interregional Biological Responses in the North Atlantic to Hydrometeorological Forcing. *Large Marine Ecosystems*, 10:27–48, dec 2002. ISSN 9780444510112. doi:10.1016/S1570-0461(02)80054-4.
- [103] P. Reid, D. Johns, M. Edwards, M. Starr, M. Poulin, and P. Snoeijs. A biological consequence of reducing Arctic ice cover: Arrival of the Pacific diatom *Neodenticula seminae* in the North Atlantic for the first time in 800000 years. *Global Change Biology*, 13:1910–1921, sep 2007. doi:10.1111/j.1365-2486.2007.01413.x.
- [104] N. Reis, N. Boiaski, and S. Ferraz. Characterization and Spatial Coverage of Heat Waves in Subtropical Brazil. *Atmosphere*, 10:284, may 2019. doi:10.3390/atmos10050284.
- [105] P. Rohini, M. Rajeevan, and A. K. Srivastava. On the Variability and Increasing Trends of Heat Waves over India. *Scientific Reports*, 6(1):26153, 2016. ISSN 2045-2322. doi:10.1038/srep26153.
- [106] P. Ruggieri, M. C. Alvarez-Castro, P. Athanasiadis, A. Bellucci, S. Materia, and S. Gualdi. North Atlantic Circulation Regimes and Heat Transport by Synoptic Eddies. *Journal of Climate*, 33(11):4769–4785, 2020. doi:10.1175/JCLI-D-19-0498.1.

- [107] S. Russo, A. Dosio, R. G. Graversen, J. Sillmann, H. Carrao, M. B. Dunbar, A. Singleton, P. Montagna, P. Barbola, and J. V. Vogt. Magnitude of extreme heat waves in present climate and their projection in a warming world. *Journal of Geophysical Research: Atmospheres*, 119(22):12, 500–512, 512, nov 2014. ISSN 2169-897X. doi:<https://doi.org/10.1002/2014JD022098>.
- [108] S. Russo, J. Sillmann, and E. M. Fischer. Top ten European heatwaves since 1950 and their occurrence in the coming decades. *Environmental Research Letters*, 10(12):124003, 2015. ISSN 1748-9326. doi:10.1088/1748-9326/10/12/124003.
- [109] K. Sato, J. Inoue, and M. Watanabe. Influence of the Gulf Stream on the Barents Sea ice retreat and Eurasian coldness during early winter. *Environmental Research Letters*, 9(8):084009, 2014. ISSN 1748-9326. doi:10.1088/1748-9326/9/8/084009.
- [110] A. A. Scaife and J. R. Knight. Ensemble simulations of the cold European winter of 2005-2006. *Quarterly Journal of the Royal Meteorological Society*, 134(636):1647–1659, oct 2008. ISSN 0035-9009. doi:<https://doi.org/10.1002/qj.312>.
- [111] B. R. Scanlon, I. Duncan, and R. C. Reedy. Drought and the water–energy nexus in Texas. *Environmental Research Letters*, 8(4):045033, 2013. ISSN 1748-9326. doi:10.1088/1748-9326/8/4/045033.
- [112] K. Schaefer, Y. Elshorbany, E. Jafarov, P. F. Schuster, R. G. Striegl, K. P. Wickland, and E. M. Sunderland. Potential impacts of mercury released from thawing permafrost. *Nature Communications*, 11(1):4650, 2020. ISSN 2041-1723. doi:10.1038/s41467-020-18398-5.
- [113] H. Schøyen and S. Bråthen. The Northern Sea Route versus the Suez Canal: cases from bulk shipping. *Journal of Transport Geography*, 19(4):977–983, 2011. ISSN 0966-6923. doi:<https://doi.org/10.1016/j.jtrangeo.2011.03.003>.
- [114] J. A. Screen and I. Simmonds. Exploring links between Arctic amplification and mid-latitude weather. *Geophysical Research Letters*, 40(5):959–964, mar 2013. ISSN 0094-8276. doi:<https://doi.org/10.1002/grl.50174>.
- [115] J. A. Screen and I. Simmonds. Amplified mid-latitude planetary waves favour particular regional weather extremes. *Nature Climate Change*, 4(8):704–709, 2014. ISSN 1758-6798. doi:10.1038/nclimate2271.
- [116] S. I. Seneviratne, T. Corti, E. L. Davin, M. Hirschi, E. B. Jaeger, I. Lehner, B. Orlowsky, and A. J. Teuling. Investigating soil moisture–climate interactions in a changing climate: A review. *Earth-Science Reviews*, 99(3):125–161, 2010. ISSN 0012-8252. doi:<https://doi.org/10.1016/j.earscirev.2010.02.004>.

- [117] A. Shabbar and B. Bonsal. An Assessment of Changes in Winter Cold and Warm Spells over Canada. *Natural Hazards*, 29(2):173–188, 2003. ISSN 1573-0840. doi:10.1023/A:1023639209987.
- [118] G. Simpkins. Extreme Arctic heat. *Nature Climate Change*, 7(2):95, 2017. ISSN 1758-6798. doi:10.1038/nclimate3213.
- [119] D. A. Smale and T. Wernberg. Extreme climatic event drives range contraction of a habitat-forming species. *Proceedings of the Royal Society B: Biological Sciences*, 280(1754):20122829, mar 2013. doi:10.1098/rspb.2012.2829.
- [120] S. A. Sorokina, C. Li, J. J. Wettstein, and N. G. Kvamstø. Observed Atmospheric Coupling between Barents Sea Ice and the Warm-Arctic Cold-Siberian Anomaly Pattern. *Journal of Climate*, 29(2):495–511, 2016. doi:10.1175/JCLI-D-15-0046.1.
- [121] C. Spensberger, E. Madonna, M. Boettcher, C. M. Grams, L. Papritz, J. F. Quinting, M. Röthlisberger, M. Sprenger, and P. Zschenderlein. Dynamics of concurrent and sequential Central European and Scandinavian heatwaves. *Quarterly Journal of the Royal Meteorological Society*, 146(732):2998–3013, oct 2020. ISSN 0035-9009. doi:https://doi.org/10.1002/qj.3822.
- [122] M. Stefanon, F. D’Andrea, and P. Drobinski. Heatwave classification over Europe and the Mediterranean region. *Environmental Research Letters*, 7(1):014023, 2012. ISSN 1748-9326. doi:10.1088/1748-9326/7/1/014023.
- [123] R. C. Sundt and W. Melle. Atlantic observation of *Calanus marshallae* (Copepoda; Calanoida). *Marine Ecology Progress Series*, 166:207–210, 1998.
- [124] K. Takaya and H. Nakamura. Mechanisms of Intraseasonal Amplification of the Cold Siberian High. *Journal of the Atmospheric Sciences*, 62(12):4423–4440, 2005. doi:10.1175/JAS3629.1.
- [125] A. M. Tomczyk and E. Bednorz. Heat waves in Central Europe and their circulation conditions. *International Journal of Climatology*, 36(2):770–782, feb 2016. ISSN 0899-8418. doi:https://doi.org/10.1002/joc.4381.
- [126] R. M. Trigo, R. García-Herrera, J. Díaz, I. F. Trigo, and M. A. Valente. How exceptional was the early August 2003 heatwave in France? *Geophysical Research Letters*, 32(10), may 2005. ISSN 0094-8276. doi:https://doi.org/10.1029/2005GL022410.
- [127] B. van den Hurk, M. Best, P. Dirmeyer, A. Pitman, J. Polcher, and J. Santanello. Acceleration of Land Surface Model Development over a Decade of Glass. *Bulletin of the American Meteorological Society*, 92(12):1593–1600, 2011. doi:10.1175/BAMS-D-11-00007.1.

- [128] G. J. Van Oldenborgh, R. Haarsma, H. de Vries, and M. Allen. Cold Extremes in North America vs. Mild Weather in Europe: The Winter of 2013–14 in the Context of a Warming World. *Bulletin of the American Meteorological Society*, 96:707–714, may 2015. doi:10.1175/BAMS-D-14-00036.1.
- [129] M. T. H. van Vliet, S. Vögele, and D. Rübhelke. Water constraints on European power supply under climate change: impacts on electricity prices. *Environmental Research Letters*, 8(3):035010, 2013. ISSN 1748-9326. doi:10.1088/1748-9326/8/3/035010.
- [130] R. Vautard, C. Honoré, M. Beekmann, and L. Rouil. Simulation of ozone during the August 2003 heat wave and emission control scenarios. *Atmospheric Environment*, 39(16):2957–2967, 2005. ISSN 1352-2310. doi:https://doi.org/10.1016/j.atmosenv.2005.01.039.
- [131] W. F. Vincent, L. G. Whyte, C. Lovejoy, C. W. Greer, I. Laurion, C. A. Suttle, J. Corbeil, and D. R. Mueller. Arctic microbial ecosystems and impacts of extreme warming during the International Polar Year. *Polar Science*, 3(3):171–180, 2009. ISSN 1873-9652. doi:https://doi.org/10.1016/j.polar.2009.05.004.
- [132] J. M. Wallace, I. M. Held, D. W. J. Thompson, K. E. Trenberth, and J. E. Walsh. Global Warming and Winter Weather. *Science*, 343(6172):729, feb 2014. doi:10.1126/science.343.6172.729.
- [133] L. Wang and W. Chen. The East Asian winter monsoon: re-amplification in the mid-2000s. *Chinese Science Bulletin*, 59(4):430–436, 2014. ISSN 1861-9541. doi:10.1007/s11434-013-0029-0.
- [134] T. Wernberg, D. A. Smale, F. Tuya, M. S. Thomsen, T. J. Langlois, T. de Bettignies, S. Bennett, and C. S. Rousseaux. An extreme climatic event alters marine ecosystem structure in a global biodiversity hotspot. *Nature Climate Change*, 3(1):78–82, 2013. ISSN 1758-6798. doi:10.1038/nclimate1627.
- [135] H. Wernli and L. Papritz. Role of polar anticyclones and mid-latitude cyclones for Arctic summertime sea-ice melting. *Nature Geoscience*, 11(2):108–113, 2018. ISSN 1752-0908. doi:10.1038/s41561-017-0041-0.
- [136] L. Woelders, J. T. M. Lenaerts, K. Hagemans, K. Akkerman, T. B. van Hoof, and W. Z. Hoek. Recent climate warming drives ecological change in a remote high-Arctic lake. *Scientific Reports*, 8(1):6858, 2018. ISSN 2045-2322. doi:10.1038/s41598-018-25148-7.

- [137] C. Woods and R. Caballero. The Role of Moist Intrusions in Winter Arctic Warming and Sea Ice Decline. *Journal of Climate*, 29(12):4473–4485, 2016. doi:10.1175/JCLI-D-15-0773.1.
- [138] C. Woods, R. Caballero, and G. Svensson. Large-scale circulation associated with moisture intrusions into the Arctic during winter. *Geophysical Research Letters*, 40(17):4717–4721, sep 2013. ISSN 0094-8276. doi:https://doi.org/10.1002/grl.50912.
- [139] T. Woollings, B. Harvey, and G. Masato. Arctic warming, atmospheric blocking and cold European winters in CMIP5 models. *Environmental Research Letters*, 9(1):014002, 2014. ISSN 1748-9326. doi:10.1088/1748-9326/9/1/014002.
- [140] B. J. Wrigley, S. Ota, and A. Kikuchi. Lightning strikes twice: Lessons learned from two food poisoning incidents in Japan. *Public Relations Review*, 32(4):349–357, 2006. ISSN 0363-8111. doi:https://doi.org/10.1016/j.pubrev.2006.09.002.
- [141] K. Ye and G. Messori. Two Leading Modes of Wintertime Atmospheric Circulation Drive the Recent Warm Arctic-Cold Eurasia Temperature Pattern. *Journal of Climate*, 33(13):5565–5587, 2020. doi:10.1175/JCLI-D-19-0403.1.
- [142] M. Zampieri, S. Russo, S. di Sabatino, M. Michetti, E. Scoccimarro, and S. Gualdi. Global assessment of heat wave magnitudes from 1901 to 2010 and implications for the river discharge of the Alps. *Science of The Total Environment*, 571:1330–1339, 2016. ISSN 0048-9697. doi:https://doi.org/10.1016/j.scitotenv.2016.07.008.
- [143] R. Zhang, C. Sun, J. Zhu, R. Zhang, and W. Li. Increased European heat waves in recent decades in response to shrinking Arctic sea ice and Eurasian snow cover. *npj Climate and Atmospheric Science*, 3(1):7, 2020. ISSN 2397-3722. doi:10.1038/s41612-020-0110-8.
- [144] P. Zschenderlein, A. H. Fink, S. Pfahl, and H. Wernli. Processes determining heat waves across different European climates. *Quarterly Journal of the Royal Meteorological Society*, 145(724):2973–2989, oct 2019. ISSN 0035-9009. doi:https://doi.org/10.1002/qj.3599.